Eur. Phys. J. C 46, 307–341 (2006)
Digital Object Identifier (DOI) 10.1140/epjc/s2006-02524-8

THE EUROPEAN PHYSICAL JOURNAL C

Searches for Gauge-Mediated Supersymmetry Breaking topologies in e^+e^- collisions at centre-of-mass energies up to $\sqrt{s} = 209\,\mathrm{GeV}$

The OPAL Collaboration

G. Abbiendi[2], C. Ainsley[5], P.F. Åkesson[3,a], G. Alexander[21], G. Anagnostou[1], K.J. Anderson[8], S. Arcelli[2], S. Asai[22], D. Axen[26], I. Bailey[25], E. Barberio[7,b], T. Barillari[31], R.J. Barlow[15], R.J. Batley[5], P. Bechtle[24], T. Behnke[24], K.W. Bell[19], P.J. Bell[1], G. Bella[21], A. Bellerive[6], G. Benelli[4], S. Bethke[31], O. Biebel[30], O. Boeriu[9], P. Bock[10], M. Boutemeur[30], S. Braibant[2], R.M. Brown[19], H.J. Burckhart[7], S. Campana[4], P. Capiluppi[2], R.K. Carnegie[6], A.A. Carter[12], J.R. Carter[5], C.Y. Chang[16], D.G. Charlton[1], C. Ciocca[2], A. Csilling[28], M. Cuffiani[2], S. Dado[20], A. De Roeck[7], E.A. De Wolf[7,c], K. Desch[24], B. Dienes[29], J. Dubbert[30], E. Duchovni[23], G. Duckeck[30], I.P. Duerdoth[15], E. Etzion[21], F. Fabbri[2], P. Ferrari[7], F. Fiedler[30], I. Fleck[9], M. Ford[15], A. Frey[7], P. Gagnon[11], J.W. Gary[4], C. Geich-Gimbel[3], G. Giacomelli[2], P. Giacomelli[2], M. Giunta[4], J. Goldberg[20], E. Gross[23], J. Grunhaus[21], M. Gruwé[7], P.O. Günther[3], A. Gupta[8], C. Hajdu[28], M. Hamann[24], G.G. Hanson[4], A. Harel[20], M. Hauschild[7], C.M. Hawkes[1], R. Hawkings[7], R.J. Hemingway[6], G. Herten[9], R.D. Heuer[24], J.C. Hill[5], D. Horváth[28,d], P. Igo-Kemenes[10], K. Ishii[22], H. Jeremie[17], P. Jovanovic[1], T.R. Junk[6,e], N. Kanaya[25], J. Kanzaki[22,f], D. Karlen[25], K. Kawagoe[22], T. Kawamoto[22], R.K. Keeler[25], R.G. Kellogg[16], B.W. Kennedy[19], K. Klein[10,g], S. Kluth[31], T. Kobayashi[22], M. Kobel[3], S. Komamiya[22], T. Krämer[24], A. Krasznahorkay[29,h], P. Krieger[6,i], J. von Krogh[10], T. Kuhl[24], M. Kupper[23], G.D. Lafferty[15], H. Landsman[20], D. Lanske[13], D. Lellouch[23], J. Letts[33], L. Levinson[23], J. Lillich[9], S.L. Lloyd[12], F.K. Loebinger[15], J. Lu[26,j], A. Ludwig[3], J. Ludwig[9], W. Mader[3,k], S. Marcellini[2], T.E. Marchant[15], A.J. Martin[12], T. Mashimo[22], P. Mättig[l], J. McKenna[26], R.A. McPherson[25], F. Meijers[7], W. Menges[24], F.S. Merritt[8], H. Mes[6,m], N. Meyer[24], A. Michelini[2], S. Mihara[22], G. Mikenberg[23], D.J. Miller[14], W. Mohr[9], T. Mori[22], A. Mutter[9], K. Nagai[12], I. Nakamura[22,n], H. Nanjo[22], H.A. Neal[32], R. Nisius[31], S.W. O'Neale[1,o], A. Oh[7], M.J. Oreglia[8], S. Orito[22,o], C. Pahl[31], G. Pásztor[4,p], J.R. Pater[15], J.E. Pilcher[8], J. Pinfold[27], D.E. Plane[7], O. Pooth[13], M. Przybycień[7,q], A. Quadt[3], K. Rabbertz[7,r], C. Rembser[7], P. Renkel[23], J.M. Roney[25], A.M. Rossi[2], Y. Rozen[20], K. Runge[9], K. Sachs[6], T. Saeki[22], E.K.G. Sarkisyan[7,s], A.D. Schaile[30], O. Schaile[30], P. Scharff-Hansen[7], J. Schieck[31], T. Schörner-Sadenius[7,t], M. Schröder[7], M. Schumacher[3], R. Seuster[13,u], T.G. Shears[7,v], B.C. Shen[4], P. Sherwood[14], A. Skuja[16], A.M. Smith[7], R. Sobie[25], S. Söldner-Rembold[15], F. Spano[8], A. Stahl[3,w], D. Strom[18], R. Ströhmer[30], S. Tarem[20], M. Tasevsky[7,x], R. Teuscher[8], M.A. Thomson[5], E. Torrence[18], D. Toya[22], P. Tran[4], I. Trigger[7], Z. Trócsányi[29,y], E. Tsur[21], M.F. Turner-Watson[1], I. Ueda[22], C.F. Vollmer[30], P. Vannerem[9], M. Verzocchi[16], C.P. Ward[5], D.R. Ward[5], P.M. Watkins[1], A.T. Watson[1], N.K. Watson[1], P.S. Wells[7], T. Wengler[7], N. Wermes[3], J.A. Wilson[1], G. Wolf[23], T.R. Wyatt[15], S. Yamashita[22], D. Zer-Zion[4], L. Zivkovic[23]

[1] School of Physics and Astronomy, University of Birmingham, Birmingham B15 2TT, UK
[2] Dipartimento di Fisica dell' Università di Bologna and INFN, 40126 Bologna, Italy
[3] Physikalisches Institut, Universität Bonn, 53115 Bonn, Germany
[4] Department of Physics, University of California, Riverside 92521, USA
[5] Cavendish Laboratory, Cambridge CB3 0HE, UK
[6] Ottawa-Carleton Institute for Physics, Department of Physics, Carleton University, Ottawa, Ontario K1S 5B6, Canada
[7] CERN, European Organisation for Nuclear Research, 1211 Geneva 23, Switzerland
[8] Enrico Fermi Institute and Department of Physics, University of Chicago, Chicago IL 60637, USA
[9] Fakultät für Physik, Albert-Ludwigs-Universität Freiburg, 79104 Freiburg, Germany
[10] Physikalisches Institut, Universität Heidelberg, 69120 Heidelberg, Germany
[11] Indiana University, Department of Physics, Bloomington IN 47405, USA
[12] Queen Mary and Westfield College, University of London, London E1 4NS, UK
[13] Technische Hochschule Aachen, III Physikalisches Institut, Sommerfeldstraße 26–28, 52056 Aachen, Germany
[14] University College London, London WC1E 6BT, UK
[15] Department of Physics, Schuster Laboratory, The University, Manchester M13 9PL, UK
[16] Department of Physics, University of Maryland, College Park, MD 20742, USA
[17] Laboratoire de Physique Nucléaire, Université de Montréal, Montréal, Québec H3C 3J7, Canada
[18] University of Oregon, Department of Physics, Eugene OR 97403, USA
[19] CCLRC Rutherford Appleton Laboratory, Chilton, Didcot, Oxfordshire OX11 0QX, UK

[20] Department of Physics, Technion-Israel Institute of Technology, Haifa 32000, Israel
[21] Department of Physics and Astronomy, Tel Aviv University, Tel Aviv 69978, Israel
[22] International Centre for Elementary Particle Physics and Department of Physics, University of Tokyo, Tokyo 113-0033, and Kobe University, Kobe 657-8501, Japan
[23] Particle Physics Department, Weizmann Institute of Science, Rehovot 76100, Israel
[24] Universität Hamburg/DESY, Institut für Experimentalphysik, Notkestraße 85, 22607 Hamburg, Germany
[25] University of Victoria, Department of Physics, P O Box 3055, Victoria BC V8W 3P6, Canada
[26] University of British Columbia, Department of Physics, Vancouver BC V6T 1Z1, Canada
[27] University of Alberta, Department of Physics, Edmonton AB T6G 2J1, Canada
[28] Research Institute for Particle and Nuclear Physics, 1525 Budapest, P O Box 49, Hungary
[29] Institute of Nuclear Research, 4001 Debrecen, P O Box 51, Hungary
[30] Ludwig-Maximilians-Universität München, Sektion Physik, Am Coulombwall 1, 85748 Garching, Germany
[31] Max-Planck-Institute für Physik, Föhringer Ring 6, 80805 München, Germany
[32] Yale University, Department of Physics, New Haven, CT 06520, USA
[33] University of California, San Diego, USA

Received: 13 June 2005 / Revised version: 9 February 2006 /
Published online: 31 March 2006 –

Abstract. Searches were performed for topologies predicted by gauge-mediated supersymmetry breaking models (GMSB). All possible lifetimes of the next-to-lightest SUSY particle (NLSP), either the lightest neutralino or slepton, decaying into the lightest SUSY particle, the gravitino, were considered. No evidence for GMSB signatures was found in the OPAL data sample collected at centre-of-mass energies up to $\sqrt{s} = 209$ GeV at LEP. Limits on the product of the production cross-sections and branching fractions are presented for all search topologies. To test the impact of the searches, a complete scan over the parameters of the minimal model of GMSB was performed. NLSP masses below 53.5 GeV/c^2 in the neutralino NLSP scenario, below 87.4 GeV/c^2 in the stau NLSP scenario and below 91.9 GeV/c^2 in the slepton co-NLSP scenario are excluded at 95% confidence level for all NLSP lifetimes. The scan determines constraints on the universal SUSY mass scale Λ from the direct SUSY particle searches of $\Lambda > 40$, 27, 21, 17, 15 TeV/c^2 for messenger indices $N = 1$, 2, 3, 4, 5 for all NLSP lifetimes.

1 Introduction

Supersymmetry (SUSY) [1] provides a method of solving the hierarchy problem by introducing a set of new particles which cancel the large radiative corrections to the Higgs mass. The cancellation is achieved by assuming that, for each standard model (SM) particle chirality state, there is one additional particle identical to its SM partner except that its spin differs by 1/2 unit. If SUSY were an exact symmetry, the new SUSY particles would have the same masses as their SM partners. Since this scenario is experimentally excluded, SUSY must be a broken symmetry. It is typically assumed that SUSY is broken in some "hidden" sector of new particles, and is "communicated" (or mediated) to the "visible" sector of SM and SUSY particles by one of the known interactions. The two scenarios for this mediation that have been most widely investigated are gravity and gauge mediation.

[a] now at CERN
[b] now at The University of Melbourne, Victoria, Australia
[c] now at University of Antwerpen, Physics Department, 2610 Antwerpen, Belgium; supported by Interuniversity Attraction Poles Programme – Belgian Science Policy
[d] and Institute of Nuclear Research, Debrecen, Hungary
[e] now at Dept. Physics, University of Illinois at Urbana-Champaign, USA
[f] and High Energy Accelerator Research Organisation (KEK), Tsukuba, Ibaraki, Japan
[g] now at RWTH Aachen, Germany
[h] and Department of Experimental Physics, University of Debrecen, Hungary
[i] now at University of Toronto, Dept. of Physics, Toronto, Canada
[j] and at TRIUMF, Vancouver, Canada
[k] now at University of Iowa, Dept of Physics and Astronomy, Iowa, USA
[l] current address Bergische Universität, Wuppertal, Germany
[m] and at TRIUMF, Vancouver, Canada V6T 2A3
[n] now at University of Pennsylvania, Philadelphia, Pennsylvania, USA
[o] Deceased
[p] and Research Institute for Particle and Nuclear Physics, Budapest, Hungary
[q] now at University of Mining and Metallurgy, Cracow, Poland
[r] now at IEKP Universität Karlsruhe, Germany
[s] and Manchester University, Manchester, M13 9PL, UK
[t] now at DESY
[u] and MPI München
[v] now at University of Liverpool, Dept. of Physics, Liverpool L69 3BX, UK
[w] now at DESY Zeuthen
[x] now at University of Antwerpen, Physics Department, 2610 Antwerpen, Belgium; supported by Interuniversity Attraction Poles Programme – Belgian Science Policy
[y] and Department of Experimental Physics, University of Debrecen, Hungary

In gauge-mediated SUSY breaking (GMSB), the hidden sector can lie at masses as low as about $10^4\,\mathrm{GeV}/c^2$. In most current GMSB theoretical work [2–4], it is assumed that this sector is coupled to a messenger sector, which in turn couples to the visible sector through normal SM gauge interactions. In its minimal version five new parameters and a sign are introduced in addition to the SM parameters, usually chosen to be the SUSY breaking scale $\sqrt{F}$, the messenger scale M, the messenger index N, the ratio of the vacuum expectation values of the two Higgs doublets $\tan\beta$, the sign of the Higgs sector mixing parameter $\mathrm{sign}(\mu)$, and the mass scale Λ, which determines the SUSY particle masses at the messenger scale.

A feature which distinguishes gravity-mediated from gauge-mediated SUSY breaking models is the mass of the gravitino, $\tilde{G}$. In gravity-mediated models, the $\tilde{G}$ is usually too heavy to have a significant effect on SUSY phenomenology, while in GMSB models the $\tilde{G}$ is typically light ($< 1\,\mathrm{MeV}/c^2$) and is the lightest SUSY particle, the LSP. While the $\tilde{G}$ is a spin 3/2 particle, only its $\pm 1/2$ spin projections (which have absorbed the goldstino associated with spontaneous SUSY breaking via the "superhiggs" mechanism [5]) interact with weak, rather than gravitational, strength interactions, and contribute to phenomenology.

In GMSB, the next-to-lightest SUSY particle (NLSP) is either the lightest neutralino, $\tilde{\chi}_1^0$ (neutralino NLSP sce-

Table 1. GMSB signatures for the stau NLSP and the slepton co-NLSP scenario. The notation (1) "prompt", (2) "within detector" and (3) "outside detector" refers to a NLSP decay such that the decay vertex is (1) close to the interaction region and not measurably displaced, (2) resolvable by the large impact parameter and kinked track searches and (3) well outside the detector. For each signature a reference to the description of the analysis is given, either to a section of this or to a separate paper

Scenario	Sparticle production (and decay)	Signal	NLSP decay	Reference
$\tilde{\tau}_1$ NLSP	$\tilde{\tau}_1^+\tilde{\tau}_1^-$	$\tau^+\tau^-\not{E}$	prompt	[7]
($\tilde{\tau}_1 \to \tau\tilde{G}$)	($\tilde{\tau}_1 \to \tau\tilde{G}$)	$\tilde{\tau} \to \tau\tilde{G}$ large I.P.	within detector	Sect. 3.2.1
		$\tilde{\tau} \to \tau\tilde{G}$ kinked tracks	within detector	Sect. 3.3.1
		$\tilde{\tau}$ tracks, high $\mathrm{d}E/\mathrm{d}x$	outside detector	[8]
	$\tilde{\chi}_1^0\tilde{\chi}_1^0$	$\tau^+\tau^-\tau^+\tau^-\not{E}$	prompt	Sect. 3.1.2
	($\tilde{\chi}_1^0 \to \tilde{\tau}_1\tau$)	$\tilde{\tau} \to \tau\tilde{G}$ large I.P.	within detector	Sect. 3.2.2
		$\tilde{\tau} \to \tau\tilde{G}$ kinked tracks	within detector	Sect. 3.3.2
		$\tilde{\tau}$ tracks, high $\mathrm{d}E/\mathrm{d}x$	outside detector	Sect. 3.4.2
	$\tilde{\chi}_1^+\tilde{\chi}_1^-$	$\tau^+\tau^-\not{E}$	prompt	[7]
	($\tilde{\chi}_1^\pm \to \tilde{\tau}_1\nu$)	$\tilde{\tau} \to \tau\tilde{G}$ large I.P.	within detector	Sect. 3.2.1
		$\tilde{\tau} \to \tau\tilde{G}$ kinked tracks	within detector	Sect. 3.3.1
		$\tilde{\tau}$ tracks, high $\mathrm{d}E/\mathrm{d}x$	outside detector	Sect. 3.4.2
	$\tilde{\mu}_\mathrm{R}^+\tilde{\mu}_\mathrm{R}^-$,	$\mu^+\mu^-\tau^+\tau^-\tau^+\tau^-\not{E}$	prompt	Sect. 3.1.2
	$\tilde{e}_\mathrm{R}^+\tilde{e}_\mathrm{R}^-$	$e^+e^-\tau^+\tau^-\tau^+\tau^-\not{E}$	prompt	Sect. 3.1.2
	($\tilde{\ell}_\mathrm{R} \to \ell\tilde{\chi}_1^0$,	$\tilde{\tau} \to \tau\tilde{G}$ large I.P.	within detector	Sect. 3.2.3
	$\tilde{\chi}_1^0 \to \tilde{\tau}_1\tau$)	$\tilde{\tau} \to \tau\tilde{G}$ kinked tracks	within detector	Sect. 3.3.3
		$\tilde{\tau}$ tracks, high $\mathrm{d}E/\mathrm{d}x$	outside detector	Sect. 3.4.2
$\tilde{\ell}_\mathrm{R}$ co-NLSP	$\tilde{\ell}_\mathrm{R}^+\tilde{\ell}_\mathrm{R}^-$	$\ell^+\ell^-\not{E}$	prompt	[7]
($\tilde{\ell}_\mathrm{R} \to \ell\tilde{G}$)	($\tilde{\ell}_\mathrm{R} \to \ell\tilde{G}$)	$\tilde{\ell} \to \ell\tilde{G}$ large I.P.	within detector	Sect. 3.2.1
		$\tilde{\ell} \to \ell\tilde{G}$ kinked tracks	within detector	Sect. 3.3.1
		$\tilde{\ell}$ tracks, high $\mathrm{d}E/\mathrm{d}x$	outside detector	[8]
	$\tilde{\chi}_1^0\tilde{\chi}_1^0$	$\ell^+\ell^-\ell^+\ell^-\not{E}$	prompt	Sect. 3.1.2
	($\tilde{\chi}_1^0 \to \tilde{\ell}_\mathrm{R}\ell$)	$\tilde{\ell} \to \ell\tilde{G}$ large I.P.	within detector	Sect. 3.2.2
		$\tilde{\ell} \to \ell\tilde{G}$ kinked tracks	within detector	Sect. 3.3.2
		$\tilde{\ell}$ tracks, high $\mathrm{d}E/\mathrm{d}x$	outside detector	Sect. 3.4.2
	$\tilde{\chi}_1^+\tilde{\chi}_1^-$	$\ell^+\ell^-\not{E}$	prompt	[7]
	($\tilde{\chi}_1^\pm \to \tilde{\ell}_\mathrm{R}\nu$)	$\tilde{\ell} \to \ell\tilde{G}$ large I.P.	within detector	Sect. 3.2.1
		$\tilde{\ell} \to \ell\tilde{G}$ kinked tracks	within detector	Sect. 3.3.1
		$\tilde{\ell}$ tracks, high $\mathrm{d}E/\mathrm{d}x$	outside detector	Sect. 3.4.2

Table 2. GMSB signatures for the neutralino NLSP scenario. The notation (1) "within detector" and (2) "outside detector" refers to a NLSP decay such that the decay vertex is (1) at the interaction region (prompt decay) up to a few tenths of centimetres inside the detector volume and (2) well outside. For each signature a reference to the description of the analysis is given, either to a section of this or to a separate paper

Scenario	Sparticle Production (and decay)	Signal	NLSP decay	Reference
$\tilde{\chi}_1^0$ NLSP	$\tilde{\chi}_1^0\tilde{\chi}_1^0$	$\gamma\gamma \not{E}$	within detector	[9]
$(\tilde{\chi}_1^0 \to \gamma\tilde{G})$	$(\tilde{\chi}_1^0 \to \gamma\tilde{G})$	$\not{E}$	outside detector	—
	$\tilde{\ell}_R^+\tilde{\ell}_R^-$	$\ell^+\ell^-\gamma(\gamma)\not{E}$	within detector	Sect. 4.1.2
	$(\tilde{\ell}_R \to \tilde{\chi}_1^0\ell)$	$\ell^+\ell^-\not{E}$	outside detector	[7]
	$\tilde{\chi}_1^+\tilde{\chi}_1^-$	$q_i\bar{q}_j q_k\bar{q}_l\gamma(\gamma)\not{E}$	within detector	Sect. 4.1.2
	$(\tilde{\chi}_1^\pm \to \tilde{\chi}_1^0 W^\pm)$	$q_i\bar{q}_j\ell^\pm\gamma(\gamma)\not{E}$	within detector	Sect. 4.1.2
		$\ell^+\ell^-\gamma(\gamma)\not{E}$	within detector	Sect. 4.1.2
		$q_i\bar{q}_j q_k\bar{q}_l\not{E}$	outside detector	[10]
		$q_i\bar{q}_j\ell^\pm\not{E}$	outside detector	[10]
		$\ell^+\ell^-\not{E}$	outside detector	[7]
	$\tilde{\chi}_1^+\tilde{\chi}_1^-$	$\ell^+\ell^-\gamma(\gamma)\not{E}$	within detector	Sect. 4.1.2
	$(\tilde{\chi}_1^\pm \to \tilde{\ell}_R\nu,$	$\ell^+\ell^-\not{E}$	outside detector	[7]
	$\tilde{\ell}_R \to \tilde{\chi}_1^0\ell)$			

nario), or the lightest scalar lepton[1], $\tilde{\ell}_1^\pm$, which is either the mass degenerate $\tilde{e}_R$, $\tilde{\mu}_R$ and $\tilde{\tau}_1$ (slepton co-NLSP scenario) or in a significant fraction of the parameter space the lightest scalar tau lepton, $\tilde{\tau}_1$ (stau NLSP scenario). For SUSY particles heavier than the NLSP, the coupling to the $\tilde{G}$ is very small, and typically they will decay to the NLSP, which then decays to the gravitino via $\tilde{\chi}_1^0 \to \gamma\tilde{G}$ or $\tilde{\ell} \to \ell\tilde{G}$.

One feature of GMSB is that the decay length $\beta\gamma c\tau$ of the NLSP depends on the intrinsic SUSY breaking scale $\sqrt{F}$:

$$\beta\gamma c\tau \propto \left(\frac{100\,\mathrm{GeV}/c^2}{m_{\mathrm{NLSP}}}\right)^5 \left(\frac{\sqrt{F}}{100\,\mathrm{TeV}}\right)^4 \left(\frac{E_{\mathrm{NLSP}}^2}{m_{\mathrm{NLSP}}^2} - 1\right)^{1/2} \mathrm{cm}\,, \quad (1)$$

where m_{NLSP} and E_{NLSP} are mass and energy of the NLSP. Due to the range allowed for $\sqrt{F}$, from $2000\,\mathrm{TeV}/c^2$ down to $100\,\mathrm{TeV}/c^2$ [6], the decay length is effectively unconstrained and decays inside and outside the detector volume have to be considered. If the NLSP decay to the gravitino occurs with a small lifetime, event signatures will include energetic leptons or photons, plus significant missing energy, $\not{E}$, due to the undetected gravitinos. For intermediate lifetimes, the events may include tracks not pointing to the primary interaction point (tracks with large impact parameters) or kinked tracks. For long lifetimes, the signatures can include tracks from heavy long-lived charged particles.

[1] For the first and second generations in the minimal GMSB model, the lighter state is predominantly right-handed, since the off-diagonal components of the mass matrix are small due to small Yukawa couplings. Therefore in the following for the selectron and the smuon the symbol $\tilde{\ell}_R$ instead of $\tilde{\ell}_1$ is often used.

In this paper, we present results on searches for GMSB signatures with either a $\tilde{\chi}_1^0$ or a $\tilde{\ell}_1$ (or $\tilde{\tau}_1$) NLSP using the data sample acquired by the OPAL detector at centre-of-mass energies of $\sqrt{s} = 189$–$209\,\mathrm{GeV}$. All relevant signatures – direct NLSP pair-production and its appearance in the decay chains of heavier SUSY particles like charginos, neutralinos or sleptons – for all NLSP lifetimes are considered in our searches. Topologies and sparticle decay modes together with a reference to the description of the analyses are given in Table 1 for the slepton and stau NLSP scenarios and in Table 2 for the neutralino NLSP scenario.

The paper is organized as follows. The OPAL detector, data and Monte Carlo samples are introduced in Sect. 2, followed by a brief description of the event selections of different topologies in the slepton and stau NLSP scenarios in Sect. 3 and for the neutralino NLSP scenario in Sect. 4. The strategy to combine such a large number of analyses is described in Sect. 5. Results are presented in Sect. 6, and finally in Sect. 7 constraints on the parameters of the minimal GMSB model are discussed.

2 Data and simulated events

A detailed description of the OPAL detector can be found elsewhere [11]. Tracking of charged particles was performed by a central detector, enclosed in a solenoid which provided a uniform axial magnetic field of 0.435 T. The central detector consisted of a two-layer silicon microvertex detector [12], a high precision vertex chamber with both axial and stereo wire layers, a large volume jet chamber providing both tracking and ionization energy loss information, and additional chambers to measure the z

Table 3. Number of observed and expected events for all searches described in this paper. The uncertainty on the expected number of events include both statistical and systematic effects. In the interpretation, results of analysis (6) at lower centre-of mass energies are used in addition. Here the numbers of observed and expected events are 0/0.01±0.00 at $\sqrt{s} = 130$ GeV, 0/0.01±0.00 at $\sqrt{s} = 161$ GeV, 0/0.01±0.00 at $\sqrt{s} = 171$ GeV and 0/0.05±0.01 at $\sqrt{s} = 183$ GeV. The numbers given in brackets in the first row of the table give the average recorded luminosity in each energy bin

Sparticle production (NLSP)	NLSP lifetime	$\langle\sqrt{s}\rangle =$ 188.7 GeV (168 pb^{-1})	$\langle\sqrt{s}\rangle =$ 191.6 GeV (30 pb^{-1})	$\langle\sqrt{s}\rangle =$ 195.5 GeV (76 pb^{-1})	$\langle\sqrt{s}\rangle =$ 199.5 GeV (78 pb^{-1})	$\langle\sqrt{s}\rangle =$ 201.6 GeV (38 pb^{-1})	$\langle\sqrt{s}\rangle =$ 205.1 GeV (74 pb^{-1})	$\langle\sqrt{s}\rangle =$ 206.7 GeV (120 pb^{-1})	$\langle\sqrt{s}\rangle =$ 208.1 GeV (8 pb^{-1})	Reference
$\tilde{\tau}_1^+\tilde{\tau}_1^-$	(1) short	1/0.93±0.56	0/0.11±0.06	1/0.25±0.13	0/0.49±0.36	0/0.18±0.28	0/0.56±0.24	1/1.13±1.02	0/0.14±0.04	Sect. 3.2.1
($\tilde{\tau}_1$)	(2) medium	0/0.71±0.31	0/0.09±0.12	0/0.22±0.33	0/0.29±0.28	0/0.17±0.18	0/0.13±0.14	0/0.21±0.22	0/0.01±0.02	Sect. 3.3.1
$\tilde{\chi}_1^0\tilde{\chi}_1^0$	(3) zero	1/1.06±0.45	0/0.15±0.11	0/0.38±0.18	0/0.31±0.17	0/0.30±0.15	0/0.24±0.15	1/0.38±0.22	0/0.03±0.04	Sect. 3.1.2
($\tilde{\tau}_1$)	(4) short	1/1.20±0.33	1/0.23±0.07	0/0.57±0.31	0/1.25±0.90	1/0.23±0.05	0/0.91±0.31	1/1.24±0.53	0/0.08±0.04	Sect. 3.2.2
	(5) medium	0/0.69±0.52	0/0.00±0.01	0/0.01±0.01	1/0.06±0.04	0/0.04±0.03	0/0.09±0.18	0/0.15±0.28	0/0.01±0.02	Sect. 3.3.2
	(6) long	0/0.07±0.05	—	0/0.08±0.02	0/0.33±0.22	0/0.04±0.01	0/0.06±0.02	0/0.11±0.04	0/0.01±0.00	Sect. 3.4.2
$\tilde{\chi}_1^+\tilde{\chi}_1^-$	short NLSP lifetime as for (1), medium lt. as for (2), long lt. as for (6)									
($\tilde{\tau}_1$)										
$\tilde{\mu}_R^+\tilde{\mu}_R^-$	(7) zero	2/1.59±0.60	0/0.22±0.13	0/0.56±0.23	1/0.46±0.20	0/0.46±0.19	1/0.35±0.20	1/0.57±0.31	0/0.05±0.05	Sect. 3.1.2
($\tilde{\tau}_1$)	(8) short	4/3.68±1.08	1/0.64±0.19	1/1.00±0.37	2/1.91±0.92	2/0.62±0.16	1/2.23±0.60	2/3.42±1.01	0/0.22±0.066	Sect. 3.2.3
	(9) medium	1/1.34±0.67	0/0.13±0.09	0/0.33±0.23	1/0.41±0.30	0/0.25±0.13	1/0.11±0.18	0/0.18±0.28	0/0.01±0.02	Sect. 3.3.3
	long NLSP lifetime as for (6)									
$\tilde{e}_R^+\tilde{e}_R^-$	zero NLSP lifetime as for (7), short lt. as for (8), medium lt. as for (9), long lt. as for (6)									
($\tilde{\tau}_1$)										
$\tilde{\ell}_R^+\tilde{\ell}_R^-$	(10) short	0/0.05±0.03	0/0.01±0.01	0/0.01±0.01	0/0.02±0.01	0/0.01±0.01	0/0.01±0.01	0/0.01±0.73	0/0.01±0.01	Sect. 3.2.1
($\tilde{\ell}_R$)	medium NLSP lifetime as for (2)									
$\tilde{\chi}_1^0\tilde{\chi}_1^0$	zero NLSP lifetime as for (3), short lt. as for (4), medium lt. as for (5), long lt. as for (6)									
($\tilde{\ell}_R$)										
$\tilde{\chi}_1^+\tilde{\chi}_1^-$	short NLSP lifetime as for (10), medium lt. as for (2), long lt. as for (6)									
($\tilde{\ell}_R$)										
$\tilde{\ell}_R^+\tilde{\ell}_R^-$	(11 A) short	0/1.97±0.45	0/0.43±0.10	0/1.02±0.24	0/1.10±0.25	0/0.45±0.11	2/1.03±0.31	1/1.62±0.48	0/0.12±0.04	Sect. 4.1.2
[(11) only]	(12 B0) short	0/0.13±0.05	0/0.03±0.01	0/0.03±0.01	0/0.04±0.01	0/0.03±0.01	0/0.16±0.05	0/0.25±0.09	0/0.02±0.00	Sect. 4.1.2
and	(12 B1) short	0/1.71±0.40	0/0.45±0.12	1/0.99±0.26	3/1.17±0.29	0/0.43±0.18	0/1.43±0.48	2/2.25±0.75	0/0.16±0.41	Sect. 4.1.2
$\tilde{\chi}_1^+\tilde{\chi}_1^-$	(12 B2) short	0/0.60±0.15	0/0.12±0.04	0/0.27±0.09	1/0.30±0.09	1/0.12±0.04	0/0.47±0.16	1/0.74±0.25	0/0.05±0.01	Sect. 4.1.2
($\tilde{\chi}_1^0$)	(12 C1) short	0/0.12±0.08	0/0.03±0.01	0/0.06±0.03	0/0.04±0.01	0/0.05±0.02	0/0.12±0.04	1/0.19±0.06	0/0.01±0.00	Sect. 4.1.2
[(11)+(12)]	(12 C2) short	2/0.60±0.15	0/0.09±0.03	0/0.25±0.07	0/0.22±0.06	0/0.16±0.04	0/0.60±0.20	0/0.95±0.32	0/0.07±0.02	Sect. 4.1.2

coordinate of tracks as they leave the central detector[2]. These detectors provided tracking coverage for polar angles $|\cos\theta| < 0.96$, with a typical transverse momentum (p_T) resolution of $\sigma_{p_T}/p_T^2 = 1.25 \times 10^{-3}\,\mathrm{GeV}/c^{-1}$. The solenoid coil was surrounded by a time-of-flight counter array and a barrel lead-glass electromagnetic calorimeter with a pre-sampler. Together with the endcap electromagnetic calorimeters, the lead-glass blocks covered the range $|\cos\theta| < 0.98$. Outside the electromagnetic calorimetry, the magnet return yoke was instrumented with streamer tubes to form a hadronic calorimeter with angular coverage in the range $|\cos\theta| < 0.91$. The region $0.91 < |\cos\theta| < 0.99$ was instrumented with an additional pole-tip hadronic calorimeter using multi-wire chambers. The detector was completed with muon detectors outside the magnet return yoke. These were composed of drift chambers in the barrel region and limited streamer tubes in the endcaps, and together covered 93% of the full solid angle.

The data used for the new particle searches described here were taken at centre-of-mass energies between 189 GeV and 209 GeV during the LEP running periods from 1998 to 2000. The total integrated luminosity is about 600 pb^{-1}, evaluated using small angle Bhabha scattering events observed in the forward calorimeters [13] with an uncertainty of about 0.3%. The data were analyzed in 8 independent bins in $\sqrt{s}$, summarized in Table 3. Large samples of Monte Carlo simulated events were generated at each $\sqrt{s}$ to optimize the search algorithms for new particles and were used to evaluate their efficiency and the number of expected events from standard model sources.

Signal events were generated for all search topologies with 10 different NLSP lifetimes ranging from a very short lifetime, $\tau = 10^{-12}$ s, corresponding to a prompt NLSP decay with a decay length of 300 μm for a particle with $\beta\gamma = p/m = 1$, up to very long lifetimes, $\tau = 10^{-6}$ s, corresponding to a stable NLSP with a decay length of 300 m which always decays outside the detector. Mass grids from 45 GeV/c^2 to the kinematic limit with 10–100 points per channel per $\sqrt{s}$ bin and 1000 events per grid point were used for the full simulation of signal Monte Carlo simulated events. The SUSYGEN [14] event generator was used to simulate the signal events for $\tilde{\ell}_R$ and $\tilde{\chi}_1^0$ pair-production. For chargino pair-production the W and Z boson widths can play an important role and are not fully treated in SUSYGEN. The DFGT generator [15] was used to simu-

[2] A right-handed coordinate system is adopted, where the x-axis points toward the centre of the LEP ring and the z-axis points in the direction of the electron beam. The polar angle θ and the azimuthal angle ϕ are defined w.r.t. z and x, respectively.

late these signal events. It includes spin correlations and allows for a proper treatment of the W boson and the Z boson width effects in the chargino decay. Both SUSYGEN and DFGT include initial-state radiation (ISR). The Lund string fragmentation scheme of PYTHIA in the JETSET package [16] was used to describe the hadronization. The gravitino mass was set to zero in the generation, since a small mass up to $\mathcal{O}$ (MeV) favoured by the models has a negligible effect on the detection efficiencies. The GEANT3 [17] software package, which was used to simulate the transport of particles through the material of the detector, only allows isotropic two- or three-body decays of long-lived particles. Thus an interface between GEANT and the event generators was created to obtain correct angular and energy distributions for the decay products of the NLSP, which decays in flight.

The simulated standard model background is composed of two-photon ($e^+e^- \to e^+e^-\gamma\gamma \to e^+e^- f\bar{f}$), four-fermion ($e^+e^- \to f\bar{f}f\bar{f}$), multi-photon ($e^+e^- \to \gamma\gamma(\gamma)$) and two-fermion ($e^+e^- \to (yZ/\gamma)^* \to l\bar{l}$ and $e^+e^- \to (Z/\gamma)^* \to q\bar{q}$) final states. Leptonic two-photon processes were simulated with the BDK [18] and Vermaseren [19] programs, and hadronic two-photon processes with the PHOJET [20] and HERWIG [21] programs. To simulate four-fermion processes, the KORALW [22] generator (which simulates ISR using a spectrum with transverse momentum) and, for final states with electrons, the grc4f [23] program (with collinear ISR) were used. Multi-photon final states were simulated with the RADCOR [24] program. For Bhabha events, the BHWIDE [25] and TEEGG [26] generators were used. Muon- and tau-pairs were simulated using the KK2F [27] program and $\nu\nu(\gamma)$ events with the NUNUGPV [28] generator. Multi-hadronic events were simulated using PYTHIA and KK2F. The equivalent luminosities of the background Monte Carlo samples were in most cases much larger than the luminosity of the data; however, in a few background samples (especially the high cross-section two-photon processes), the equivalent luminosity of the background Monte Carlo was only about $2\times$ that of the data. Final states with six or more primary fermions were not included in the background Monte Carlo samples but they are expected to make a negligible contribution.

The simulated signal and background samples were processed through the full simulation of the detector, and the same analysis chains were applied to Monte Carlo simulated events as to the data. The full Poisson statistical uncertainties on the signal and background Monte Carlo are included in all results, although Gaussian errors are used in illustrative plots and tables. All search analyses described in this paper used the same sets of simulated background events.

3 Searches in the stau NLSP and slepton co-NLSP scenarios

In the scenarios where mass-degenerate charged sleptons or the stau are the next-to-lightest SUSY particles, they decay to their charged Standard Model partner and the electrically neutral, lightest SUSY particle, the gravitino. Depending on the NLSP lifetime, different analyses were applied. In the following section all searches for SUSY particles in the stau NLSP and the slepton co-NLSP scenario are presented. In Table 3 all search results not described in other papers are summarized.

3.1 Searches for promptly decaying charged NLSPs

The decay vertex of an NLSP with a lifetime less than 10^{-11} s is close to the interaction region and considered not to be displaced from the primary vertex. Depending on whether the NLSP is directly pair-produced or appears in the decay chain of heavier SUSY particles, two or more charged leptons are expected in an event and different search algorithms were optimized to select candidate events with different track multiplicities.

3.1.1 Search for di-lepton events with missing transverse momentum

Candidate events for pair-produced NLSPs, decaying promptly into a lepton and a gravitino ($e^+e^- \to \tilde{\ell}^+_{\mathrm{R}}\tilde{\ell}^-_{\mathrm{R}}$, $\tilde{\ell}_{\mathrm{R}} \to \ell\tilde{G}$), should have the signature of two leptons plus missing transverse momentum. The search for events of this type is described in [7]. The number of di-lepton events, the dependence on centre-of-mass energy and the event properties are consistent with expectations from standard model processes, predominantly $\mathrm{W}^+\mathrm{W}^-$ production with both W bosons decaying leptonically. No evidence for new phenomena is apparent. The topology of two leptons plus missing transverse momentum can also result from the pair-production of charginos which decay to an invisible neutrino and the charged NLSP ($e^+e^- \to \tilde{\chi}^+_1\tilde{\chi}^-_1$, $\tilde{\chi}^\pm_1 \to \tilde{\ell}_{\mathrm{R}}\nu$, $\tilde{\ell}_{\mathrm{R}} \to \ell\tilde{G}$). Thus the same analysis as for pair-produced NLSPs is applied.

3.1.2 Selection of events with more than two leptons and missing energy

The NLSP might appear in the decay chain of a heavier pair-produced SUSY particle, a neutralino or a heavy slepton. In such cases in addition to the two leptons from the prompt decays of both NLSPs, two or four more leptons are expected in the detector ($e^+e^- \to \tilde{\chi}^0_1\tilde{\chi}^0_1$, $\tilde{\chi}^0_1 \to \tilde{\ell}_{\mathrm{R}}\ell$, $\tilde{\ell}_{\mathrm{R}} \to \ell\tilde{G}$ or $e^+e^- \to \tilde{\ell}^+_{\mathrm{R}}\tilde{\ell}^-_{\mathrm{R}}$, $\tilde{\ell}_{\mathrm{R}} \to \ell\tilde{\chi}^0_1$, $\tilde{\chi}^0_1 \to \tau\tilde{\tau}$, $\tilde{\tau} \to \tau\tilde{G}$).

An analysis to search for such topologies with multi-leptons and missing energy which performs no explicit electron or muon identification was designed to maintain simplicity, minimize systematic uncertainties and maximize efficiency for all lepton flavours. After the event reconstruction, double-counting of energy between tracks and calorimeter clusters was corrected by reducing the calorimeter cluster energy by the expected energy deposition from aligned charged tracks [29], including particle identification information. Charged tracks and neutral clusters were defined to be of "good" quality using the requirements of [29].

The analysis was split into three steps:

1. preselection of events with low to intermediate multiplicity and missing energy;
2. additional kinematic requirements to remove unmodeled backgrounds;
3. requirements that each event contains at least four jets, each consistent with being an isolated lepton (including a tau).

(1) Preselection.

(P1) The number of good charged tracks N_{trk} in the event satisfied $4 \leq N_{\mathrm{trk}} \leq 10$. This cut removed a large fraction of the lepton pair and multihadronic backgrounds.

(P2) Events that may include charged tracks originating from noise in the central jet chamber were removed by vetoing events containing any tracks with $\mathrm{d}E/\mathrm{d}x < 5\,\mathrm{keV/cm}$.

(P3) $N_{\mathrm{trk}}/N_{\mathrm{trk}}^{\mathrm{tot}} > 0.20$, where $N_{\mathrm{trk}}^{\mathrm{tot}}$ is the total number of charged tracks reconstructed in the event. This reduced the number of events due to machine backgrounds (e.g. beam-gas and beam-wall interactions).

(P4) Cosmic rays were vetoed using information from the tracking and time-of-flight systems using the cuts described in [10].

(P5) $M_{\mathrm{vis}} > 5.0\,\mathrm{GeV}/c^2$, where M_{vis} is the visible mass of the event. This cut was required to remove events which were not simulated in the untagged two-photon Monte Carlo generation.

(P6) $P_{\mathrm{T,miss}} > 0.05 \times \sqrt{s}$, where $P_{\mathrm{T,miss}}$ is the magnitude of the component of event momentum transverse to the beam axis. This greatly reduced the number of two-photon and two-fermion events.

(P7) Cuts were made on the maximum energy deposited in either side of the forward calorimeters in order to reduce two-photon and some machine backgrounds. These cuts have an associated efficiency loss due to activity which may be present in these subdetectors for signal (or background) events, which was evaluated with random beam-crossing triggers. The typical efficiency loss was about 3%.

(2) Kinematic requirements. There is an excess of events surviving the preselection. This excess does not have the characteristics of any of the signal hypotheses consid-

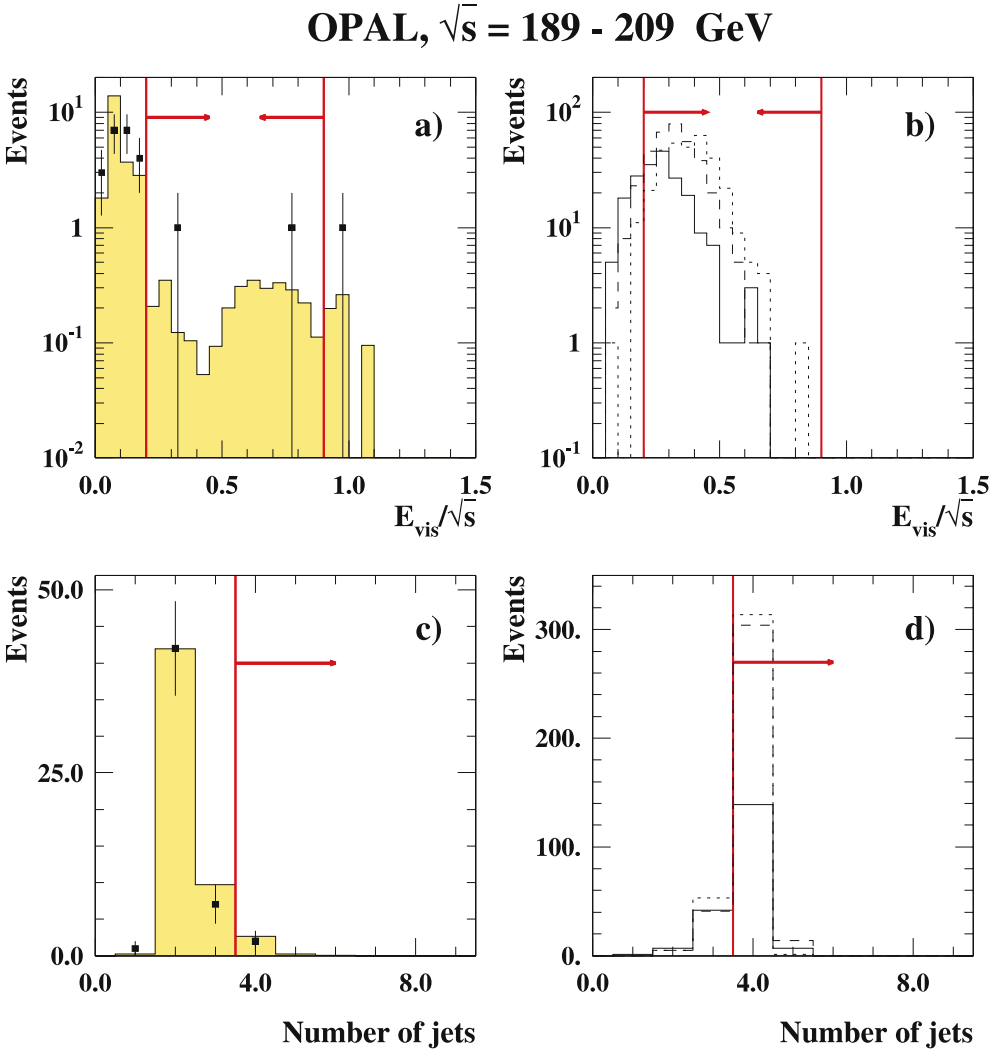

Fig. 1. Distributions of the event visible energy (**a, b**) and the number of low multiplicity jets consistent with having originated from leptons (**c, d**) in the search for multi-leptons with missing energy described in Sect. 3.1.2. The distributions are plotted with all other cuts applied. In **a** and **c** the *points* represent the selected data events from the entire 189–209 GeV data sets, while the *shaded regions* show the expectation from standard model backgrounds. Plots **b** and **d** show examples of distributions with arbitrary scale for signal events for $e^+e^- \to \tilde{\chi}_1^0\tilde{\chi}_1^0 \to \tilde{\tau}\tau\tilde{\tau}\tau$ with the prompt decay $\tilde{\tau} \to \tau\tilde{G}$ at $\sqrt{s} = 206.0\,\mathrm{GeV}$. The *solid, dashed* and *dotted lines* correspond to $(\tilde{\chi}_1^0, \tilde{\tau})$ mass combinations of (50,45), (85,65) and (102,45) GeV/c^2, respectively. The *arrows* indicate the cut positions

ered in this paper, and it was removed with the following requirements.

(K1) $\phi_{\rm acop} > 10^\circ$. The acoplanarity angle $\phi_{\rm acop}$ was calculated by forcing the event into two jets using the Durham jet finder [30], and subtracting the opening angle between the two jets in the plane transverse to the beam axis from 180°.

(K2) $|\cos\theta_{\rm miss}| < 0.90$, where $\theta_{\rm miss}$ is the polar angle of the event missing momentum vector.

(K3) $0.20 < E_{\rm vis}/\sqrt{s} < 0.90$ where $E_{\rm vis}$ is the event visible energy. The distributions of the event visible energy in data and simulated background are illustrated in Fig. 1a and b.

(3) Lepton-jet identification. The events surviving the preselection and kinematic requirements were split up into jets. The jets were then required to be consistent with having originated from electrons, muons, or tau-leptons. The signal hypotheses considered here are most often dominated by tau-leptons, and no explicit electron or muon identification tools are used. The event was split into jets using the Durham jet finder with a jet resolution parameter $y_{\rm cut}$ [30] of 0.0004. This $y_{\rm cut}$ was chosen as the smallest value (to maximize efficiency for finding leptons which are close to each other) which would not split single 3-prong tau-lepton jets into multiple jets. The following cuts were then applied.

(1) $N_{\ell\text{-jet}} \geq 4$, where $N_{\ell\text{-jet}}$ is the number of jets in the event compatible with being from a parton-level lepton:
   - Lepton-jet momentum satisfies $0.01 \leq P_{\ell\text{-jet}} < / E_{\rm beam} \leq 0.80$;
   - Lepton-jet mass satisfies $M_{\ell\text{-jet}} \leq 5\,{\rm GeV}/c^2$;
   - Number of charged tracks satisfies $1 \leq N_{\rm trk} \leq 3$.

   The distributions of the number of lepton-jets in data and simulated background are illustrated in Fig. 1c and d.

(2) $\theta_{\rm isol} > 10^\circ$ where $\theta_{\rm isol}$ is the smallest opening angle between any two lepton-jets.

(3) $\Sigma|\cos\theta_{\ell\text{-jet}}| \leq 3$, where $\Sigma|\cos\theta_{\ell\text{-jet}}|$ is the sum of the magnitudes of the cosines of the polar angles of the lepton-jet candidates. This cut removed a small residual amount of $e^+e^- \to q\bar{q}$ background.

(4) $E_{\rm sum}({\rm non}\ell\text{-jet})/E_{\rm vis} < 0.20$, where $E_{\rm sum}({\rm non}\ell\text{-jet})/E_{\rm vis}$ is the fraction of the event visible energy which is not contained in a lepton-jet candidate.

The full analysis retains efficiency for the GMSB processes $\tilde{\chi}^0_1\tilde{\chi}^0_1 \to \tilde{\ell}\ell\tilde{\ell}'\ell'$, both for the case where the neutralino decays with equal branching ratios into all three slepton generations (equal BR), and also when it decays to $\tilde{\tau}\tau$ with a 100% branching fraction. Typically when the mass difference $M(\tilde{\chi}^0_1) - M(\tilde{\ell})$ is above $5\,{\rm GeV}/c^2$, the efficiency for the equal BR scenario is 40%–50%, while for the 100% $\tilde{\tau}\tau$ decay it is 30%–40%. For $M(\tilde{\chi}^0_1) - M(\tilde{\ell}) = 5\,{\rm GeV}/c^2$, the corresponding efficiencies are typically 30% and 15%. For $M(\tilde{\chi}^0_1) - M(\tilde{\ell})$ as low as $2\,{\rm GeV}/c^2$, the equal BR scenario retains about 10% efficiency, while the very soft recoil tau leptons make the 100% $\tilde{\tau}\tau$ BR have about 1% efficiency. The full selection yields two events in the data with $2.8 \pm 0.3({\rm stat})^{+0.9}_{-0.3}({\rm syst})$ expected from the background.

To search for selectron and smuon pair-production, the final analysis cut (on the fraction of energy in the event which is not included in a lepton candidate jet) has relatively poor efficiency. This is due to the six leptons in the event, any of which could fail the lepton-jet classification. The optimal search for that process therefore excludes the final cut, and selects five events in the data with $4.2 \pm 0.3({\rm stat})^{+1.4}_{-0.4}({\rm syst})$ expected in the background. The mass grid in this mode is three dimensional, since the decay proceeds via $\tilde{\ell} \to \ell\tilde{\chi}^0 \to \ell\tilde{\tau}\tau$, and therefore the neutralino mass is also important with the efficiency depending strongly on both $M(\tilde{\ell}) - M(\tilde{\chi}^0_1)$ and $M(\tilde{\chi}^0_1) - M(\tilde{\tau})$. The detection efficiency for $\tilde{e}^+\tilde{e}^-$ and $\tilde{\mu}^+\tilde{\mu}^-$ are similar, with the $\tilde{\mu}^+\tilde{\mu}^-$ process always slightly higher. If all mass differences in the process are $> 5\,{\rm GeV}/c^2$, the detection efficiencies are about 50%. For $M(\tilde{\ell}) - M(\tilde{\chi}^0_1)$ as low as $2\,{\rm GeV}/c^2$ (soft electrons or muons) the efficiency is about 35%–45%, while for $M(\tilde{\chi}^0_1) - M(\tilde{\tau})$ as low as $2\,{\rm GeV}/c^2$ (soft taus) the efficiency is typically reduced to about 15%.

3.1.2.1 Systematic uncertainties. The dominant background in the selection is from non-multiperipheral 4-fermion production (which in our simulations is almost entirely due to the production of four charged leptons), constituting 80% of the total background expectation. A smaller contribution of about 15% is expected from the multiperipheral diagrams $e^+e^- \to e^+e^-\ell^+\ell^-$ (about 95% from $e^+e^- \to e^+e^-\tau^+\tau^-$). The remaining 5% is from $e^+e^- \to \tau^+\tau^-$. All other background processes are negligible. The Monte Carlo modeling of the background was tested using different event generators. Of particular concern is the fact that, in our principal background samples available at all centre-of-mass energies, the multiperipheral diagrams are treated with specialized "two-photon" event generators, which neglect interference with non-multiperipheral diagrams. Special samples of the full set of $e^+e^- \to e^+e^-\ell^+\ell^-$ diagrams, including interference, were prepared using grc4f2.2 [23] at $\sqrt{s} = 206\,{\rm GeV}$ to study this effect. The background using the full set of $e^+e^-\ell^+\ell^-$ diagrams including interference changes by $(-41 \pm 5)\%$ after the preselection compared to using our standard set of Monte Carlo generators. After all cuts, the result is $(+20 \pm 20)\%$. The systematic uncertainty for this effect is taken to be 40% on the $e^+e^-\ell^+\ell^-$ component of the background. The modeling of the 4-fermion background, excluding $e^+e^-\ell^+\ell^-$, was tested by comparing grc4f to our primary event generator KORALW4f. After the preselection, the background from grc4f changes by $(+11 \pm 4)\%$, while after all cuts it changes by $(-10 \pm 30)\%$. A 10% systematic uncertainty is assigned to the non $e^+e^-\ell^+\ell^-$ 4-fermion background from this check. The modeling of $e^+e^- \to \tau^+\tau^-$ was checked comparing the predictions of KK2f and KoralZ. The difference was negligible ($< 1\%$) and it is neglected.

The modeling of the cut variables by the detector simulation can introduce additional systematic uncertainties.

This modeling was checked by comparing data samples with "relaxed cuts", in which any signal contribution is expected to be negligible, with simulated background to determine the uncertainty on each cut variable. Each cut position was varied in each direction by this uncertainty, and the background level and signal efficiency re-evaluated. The lepton-jet identification was checked using different jet finders and jet resolution parameters, but there was no indication for any systematic bias from that procedure and no additional uncertainties are assigned. From these studies, the systematic uncertainty on the background due to the Monte Carlo modeling of the cut variables is taken as $+31.5/-5.6\%$, and on the relative signal efficiency as $+4.2/-4.0\%$, which is symmetrised to $\pm 4\%$.

3.2 Searches for charged NLSPs with short lifetime (tracks with large impact parameters)

If the NLSP is a slepton and its lifetime is such that the decay happens within a few centimetres of the primary interaction point, no NLSP track can be reconstructed. Only secondary tracks of its decay products are visible and they have large impact parameters with respect to the primary interaction point. In the following section the analyses searching for large impact parameter tracks consistent with short-lived NLSPs with lifetimes between roughly 10^{-11} s and 10^{-9} s are discussed.

All search topologies expected from SUSY particles in the stau or slepton co-NLSP scenarios have in common that, for short NLSP lifetimes, at least two tracks with large impact parameters would be present. The number of additional tracks depends on the pair-produced SUSY particle. The number of good tracks [29] in the event was determined, and then all tracks in the event were classified into one of three categories.

- Primary tracks: Good tracks with a distance from the point of closest approach to the event vertex in the x–y plane, the impact parameter $|d_0|$, smaller than 0.05 cm.
- Secondary tracks: Good tracks with an impact parameter $|d_0|$ greater than 0.05 cm, a high impact parameter precision of $\delta d_0/|d_0| < 0.1$ and a significant amount of transverse momentum ($p_{\mathrm{T}} > 1.5\,\mathrm{GeV}/c$).
- Additional tracks: All remaining tracks.

Candidate events must contain at most ten good tracks and at least two secondary tracks.

3.2.1 Event selection for direct NLSP and chargino pair-production

For a smuon or selectron NLSP, the processes $e^+e^- \to \tilde{\ell}_{\mathrm{R}}^+\tilde{\ell}_{\mathrm{R}}^-$ and $e^+e^- \to \tilde{\chi}_1^+\tilde{\chi}_1^-$ ($\tilde{\chi}_1^\pm \to \tilde{\ell}_{\mathrm{R}}\nu$) followed by the delayed decay of the NLSP ($\tilde{\ell}_{\mathrm{R}} \to \ell\tilde{G}$) would lead to a signature of two tracks in the event, both of which can have large impact parameters.

(1) It was required that exactly two secondary tracks, no primary tracks and no more than three additional tracks were found.

After this topological cut, a selection was applied to separate the signal from the background, mainly two-photon or (radiative) Bhabha events, cosmic particles traversing the detector, hadronic interactions with the detector material or beam wall and beam gas events.

(2) To reduce combinatorial background, the two secondary tracks were required to have different charges to satisfy charge conservation.
(3) The barrel time-of-flight detector and the central jet chamber were used to reject cosmic ray particles.
(4) To reduce the background from beam-gas events, which often contain tracks coming from an interaction point that is shifted by a large amount along the z-axis with respect to the main event vertex, the longitudinal impact parameter z_0 of each secondary track was required to satisfy $|z_0| < 40$ cm. If both tracks had a $|z_0|$ greater than 6 cm, the longitudinal impact parameters z_0 of the two tracks were required to have opposite signs.
(5) To reject background containing back-to-back tracks, especially Bhabha events and muon pairs, the angle $\Delta\phi$ in the x–y plane between the two secondary tracks was required to satisfy $5^\circ < \Delta\phi < 175^\circ$.
(6) To reduce the remaining background from two–photon events, each secondary track must have had a total momentum $p > 10\,\mathrm{GeV}/c$.
(7) To reduce the two-photon background, the invariant mass W of the two selected secondary tracks, which were assumed to be pions, was required to satisfy $W > 5\,\mathrm{GeV}/c^2$.

For pair-produced smuons, selection efficiencies in the range of 60%–70% were achieved. As selectrons would have been produced in the t-channel, leading to an enhanced production in the direction of the initial particle beams, selection efficiencies for selectrons range between 30%–65%. Efficiencies for chargino pair-production and decays to a smuon or selectron are in the range of 35%–43%. This efficiency is lower than for directly produced smuons or selectrons as additional visible energy is taken away by the neutrino from the chargino decay. In the whole data set no event was selected by the analysis, in agreement with the $0.13 \pm 0.03_{\mathrm{stat.}} \pm 0.73_{\mathrm{syst.}}$ events expected from standard model sources.

If the pair-produced NLSP is a stau or if the pair-produced chargino decays into a neutrino and the stau, the lepton in the event is a tau. As the tau decays to one or more charged particles plus a neutrino, additional energy is missing from the event. To take this into account, relaxed cuts were used for searches in the stau NLSP scenario.

(6*) At least one of the secondary tracks must have had a momentum $p \geq 5\,\mathrm{GeV}/c$.
(7*) The invariant mass of the two secondary tracks was required to be at least $3\,\mathrm{GeV}/c^2$.

The efficiency for pair-produced staus ranges between 45% and 50%. For charginos in the stau NLSP scenario the efficiency ranges from 38% up to 48% and is a bit lower than for direct stau production because of additional missing energy from the neutrino from the chargino decay.

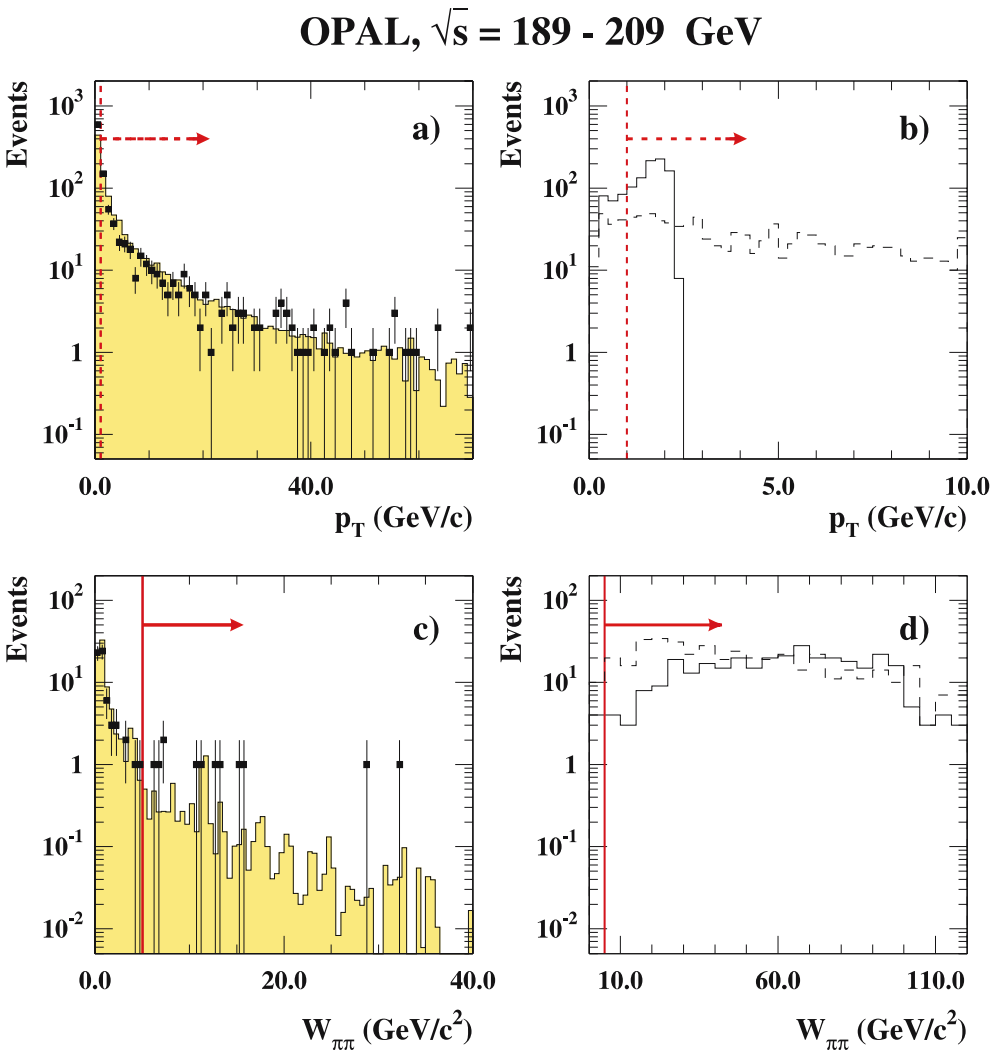

Fig. 2. Distributions of variables in the search for charged NLSPs with medium lifetime (tracks with large impact parameters) before a specific selection cut. The particular examples were taken from the search for neutrino pair-production, Sect. 3.2.2. The data, taken at centre-of-mass energies of 189–209 GeV are represented by dots, the simulated background from standard model sources by a shaded histogram. Plot **a** shows the distribution of the transverse momentum p_{T} of the primary tracks before cut (3). Events with at least two primary tracks with a momentum p_{T} greater than 1.0 GeV/c are selected. The value is indicated by a *hatched line* and *arrow*. Plot **c** gives the invariant mass $W_{\pi\pi}$ of the secondary tracks assuming a decay into two charged pions before cut(5). The *arrow* gives the region which is selected by the analysis. In **b** and **d** the *solid* and *dashed lines* indicate the distributions with arbitrary normalization for an expected signal which corresponds to $(\tilde{\chi}_1^0,\ \tilde{\tau}_1^{\pm})$ mass combinations of (102, 100) and (50, 45) GeV/c^2

After all cuts there were three events left in the data, while $3.79 \pm 0.57_{\mathrm{stat.}} \pm 1.14_{\mathrm{syst.}}$ events are expected from simulated standard model sources.

3.2.2 Event selection for neutralino pair-production

Pair-produced neutralinos are produced and decay via the processes $e^+e^- \to \tilde{\chi}_1^0\tilde{\chi}_1^0$, $\tilde{\chi}_1^0 \to \tilde{\ell}_{\mathrm{R}}\ell$ and $\tilde{\ell}_{\mathrm{R}} \to \ell\tilde{G}$ with the ℓ a tau, muon or electron. Thus in this channel there are four leptons in the final state, two of which might have large impact parameters depending on the slepton NLSP lifetime. The cuts to search for such events were

(1) events with at least two secondary tracks and at least two primary tracks were selected. No cut on the number of additional tracks was imposed.
(2) For all secondary tracks the longitudinal impact parameter $|z_0|$ was required to satisfy $|z_0| \leq 40$ cm to reduce cosmic particles, beam wall and beam gas events.
(3) At least two of the primary tracks must have had a transverse momentum larger than 1 GeV/c. The transverse momenta of the primary tracks for the data and the simulated background before this cut are shown in Fig. 2. Apart from the poorly modeled very low–momentum region, mainly consisting of two-photon events, good agreement is found. After the cut, 158 events remained in the data samples recorded at centre-of-mass energies between 189 GeV and 209 GeV, with 186.4 events expected from standard model sources. Additionally at least two primary tracks were required to have had hits in the silicon microvertex detector and the vertex chamber.
(4) For Bhabha events the two primary tracks are usually back-to-back. To reject this background, the opening angle between all pairs of primary tracks φ in the x–y plane was required to satisfy $\varphi \leq 176°$.
(5) To separate the signal from the remaining two-photon background, the invariant mass W of all secondary tracks was required to fulfill $W > 5$ GeV/c^2. In Fig. 2 the distributions of the invariant mass before the cut are shown for data and simulated background. After the cut, 12 events remained in the entire data sample, with 9.0 events expected from the background sources.
(6) Secondary particles can also be produced in photon conversions. In this case their tracks often start in the middle of the jet chamber and have, due to the

boost in the forward direction, relatively small impact parameters. For the signal, secondary particles arise from the decay of heavy SUSY particles, resulting in a much smaller boost. Thus to produce equally small impact parameters the flight lengths of the primary particles must be much shorter than for photons, and the secondary tracks start, in general, at radii smaller than those of the jet chamber. To veto such tracks from photon conversions the following cut was applied: for tracks with an impact parameter $|d_0| < 2$ cm, the first hit wire in the jet chamber must have been measured at a radial distance to the primary interaction point of less than 40 cm.

(7) Finally, to reduce remaining background from two-fermion and multi-hadronic events, the vector sum of the transverse momenta of all secondary tracks was required to exceed 3 GeV/c.

Selection efficiencies are around 50% in the slepton co-NLSP scenario and 35% in the stau NLSP scenario. In total four events were left in the data in good agreement with $5.71 \pm 1.15_{\text{stat.}} \pm 0.29_{\text{syst.}}$ events expected from simulated standard model background sources.

3.2.3 Event selection for selectron or smuon pair-production (stau NLSP)

The production and decay of selectrons or smuons following $e^+e^- \to \tilde{\ell}^+_{\text{R}}\tilde{\ell}^-_{\text{R}}$, $\tilde{\ell}_{\text{R}} \to \ell\tilde{\chi}^0_1$, $\tilde{\chi}^0_1 \to \tau\tilde{\tau}$ and $\tilde{\tau} \to \tau\tilde{G}$, leads to a final state with six leptons. In the event, two primary electrons or muons, two primary taus and finally two secondary taus and their decay products, which – depending on the NLSP lifetime – can have large impact parameters, are expected and the following cuts are used.

(1) For a candidate event, at least two secondary and at least three primary tracks were required. No cut on the number of additional tracks was applied.

(2) For all secondary tracks the longitudinal impact parameter $|z_0|$ was required to satisfy $|z_0| \leq 40$ cm to reduce cosmic particles, beam wall and beam gas events.

(3) At least two of the primary tracks must have had a transverse momentum larger than 1 GeV/c to reduce the background, mainly from two-photon events. Additionally at least two primary tracks must have had hits in the silicon microvertex detector and the vertex chamber.

(4) The invariant mass W calculated from all secondary tracks was required to be larger than 5 GeV/c^2 to remove remaining background from two-photon events.

(5) To veto photon conversions the radius of the innermost hit wire in the central jet chamber associated to tracks with $|d_0| < 2$ cm was required to be smaller than 40 cm, as described for cut (6) in Sect. 3.2.2.

Selection efficiencies of 45% for both selectron and smuon pair-production are reached. In the entire data set, 13 events survived the selection, which is in good agreement with $13.72 \pm 1.74_{\text{stat.}} \pm 0.77_{\text{syst.}}$ events that are expected from standard model background sources.

3.2.4 Statistical and systematic uncertainties

The statistical uncertainties on the number of expected background events due to the limited amount of simulated data reach 50% for single centre-of-mass energies mainly because of the limited number of simulated two-photon events, which are expected to have high production cross-sections of the order of 10 nb.

Most cuts applied in the search for tracks with large impact parameters rely on the tracking performance of the detector. If the resolution of the track parameters in the detector simulation is different from the one in the recorded data, this can lead to systematic effects on the number of expected background events. Therefore, to obtain a conservative estimation of the size of this effect, the resolution of the track parameters was degraded (smeared) by 10% in the x–y plane and by 40% in the z direction. With the smeared track parameters all analyses were repeated on the simulated background samples. The absolute differences to the background numbers without smearing were taken as the systematic uncertainties. For analyses with a very small number of expected SM events, the uncertainties can reach 100% for single centre-of-mass energies. But in general systematic effects were found to be smaller than statistical uncertainties.

3.3 Searches for charged NLSPs with medium lifetime (kinked tracks)

The discovery signals for charged NLSPs with a lifetime in the range of about $10^{-9}\,\text{s} < \tau < 10^{-7}\,\text{s}$ are spectacular, with a kinked track in the tracking chambers. A kinked track is defined by the presence of a primary and at least one secondary track segment which intersect inside the sensitive volume of the central tracking chamber. In this analysis, all tracks reconstructed in the central tracking system are considered.

Primary tracks: tracks originating at the interaction point of the event, traverse through the tracking detector volume with a minimum transverse momentum of 110 MeV/c with no signal in the outer detectors.

Secondary tracks: A minimum transverse momentum of 110 MeV/c with $|d_0|$ greater than 2.5 cm and no associated hit in the silicon detector.

A kink candidate is found if there is an intersection point, the kink vertex, between the helices which describe the track curvature of the primary and secondary track candidates in the plane transverse to the beam axis. If the kink vertex is within the detector volume, its position along the beam axis is determined more precisely by refitting the two tracks assuming a common intersection point. After the refit the vertex has still to be within the detector volume. Further cuts reduce the combinatoric background. The position of the last hit on the primary track measured in the track direction must not be more than 10 cm before nor more than 5 cm beyond kink vertex. Similarly, the first hit on the secondary track must not be located more than 5 cm in front of the vertex. The uncertainty on the refitted position along the beam axis must be less than 4 cm

and the adjustment of the cosine of the track angle with respect to the beam axis by the refit has to be less than 0.1 for the primary track and less than 0.15 for the secondary track.

No selection cut was placed on the specific ionization energy loss $\mathrm{d}E/\mathrm{d}x$ of the primary heavy charged particle, in order to keep the kinked track search independent from the searches for heavy stable charged particles. For the latter, the measurement of the $\mathrm{d}E/\mathrm{d}x$ was the main tool.

Depending on whether the NLSP was directly pair-produced or appeared in the decay chain of other SUSY particles, the kinked tracks would be accompanied by up to four additional charged leptons; thus, different search algorithms were designed and optimized for the different track multiplicities in the event.

3.3.1 Event selection for direct NLSP and chargino pair-production

The processes $e^+e^- \to \tilde{\ell}^+_{\mathrm{R}}\tilde{\ell}^-_{\mathrm{R}}$ and $e^+e^- \to \tilde{\chi}^+_1\tilde{\chi}^-_1$ $(\tilde{\chi}^\pm_1 \to \tilde{\ell}_{\mathrm{R}}\nu)$ followed by the delayed decay of the NLSP lead to a signature of two tracks in the event of which one or both can have a kink. To be selected as an event consistent with this topology the following criteria have to be satisfied:

(1) At least one kink vertex in the event.
(2) The sum of the numbers of primary plus secondary tracks must be less than or equal to 20 and the number of good tracks [29] should not exceed five.
(3) There must not be more than two primary track candidates and the scalar sum of their transverse momenta p_{T} had to be greater than $4\,\mathrm{GeV}/c$ to reject events from two-photon processes.
(4) The kink vertex had to be within the geometrical acceptance of the central jet chamber: $r \leq 181.5\,\mathrm{cm}$ and $|z| \leq (0.5 \cdot [153.288\,\mathrm{cm} + (r - 24.5\,\mathrm{cm}) \cdot \tan(15^\circ) \cdot \cos(7.5^\circ)] - 1.0)$.
(5) The momentum of the secondary track had to satisfy $p \geq 1\,\mathrm{GeV}/c$ and must not be parallel to a wire in the jet chamber to within 1° to remove combinatoric background and poorly measured tracks.
(6) The transverse momentum p_{T} of the primary track had to satisfy $p_{\mathrm{T}} \geq 1\,\mathrm{GeV}/c$. Figure 3a shows the distribution of the transverse momentum of the primary track. Unmodeled background events at momenta less

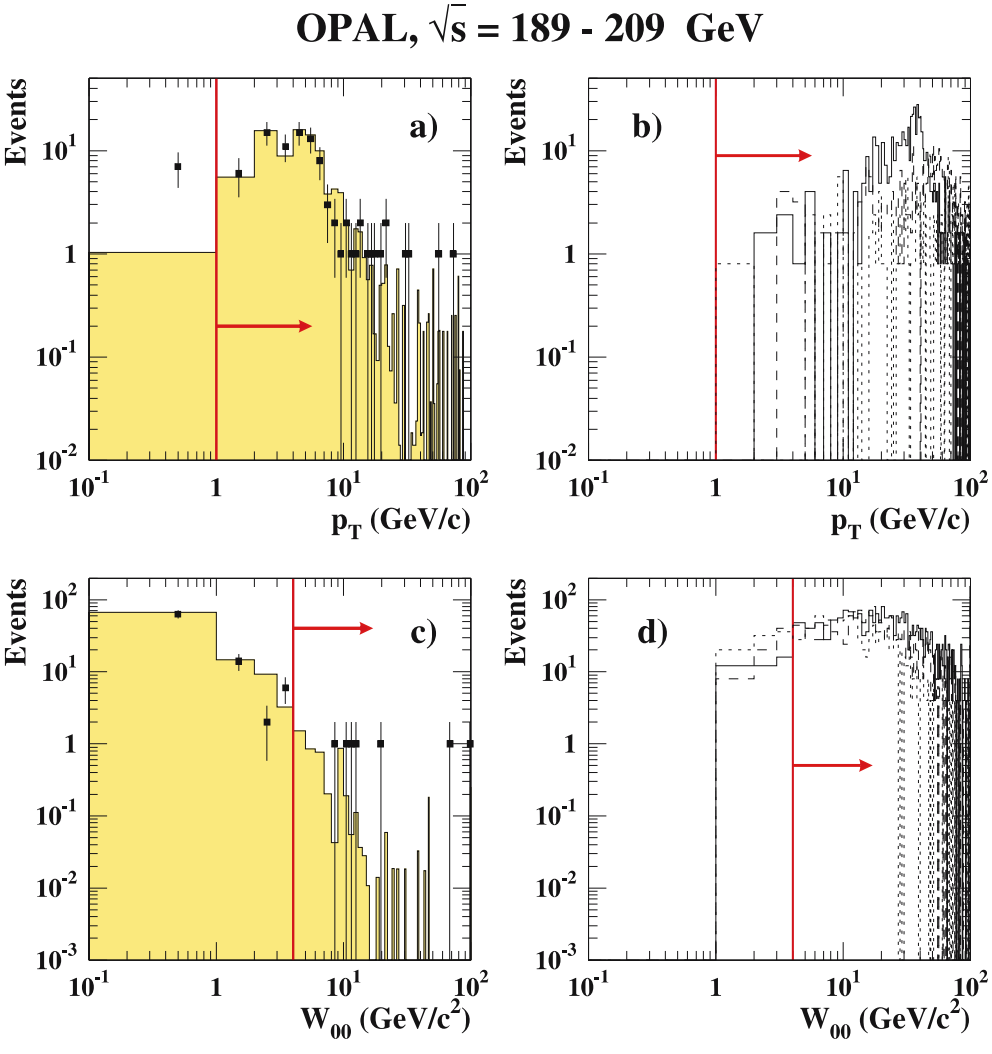

Fig. 3. Distributions of variables in the search for charged NLSPs with medium lifetime (*kinked tracks*) before a specific selection cut. The particular examples were taken from the search for direct NLSP pair-production, Sect. 3.3.1. The data, taken at centre-of-mass energies of 189–209 GeV are represented by *dots*, the simulated background from standard model sources by a *shaded histogram*. In (**b**, **d**) the *solid, dashed* and *dotted lines* indicate the distributions expected from a pair-produced stau with masses of 65, 80 and $95\,\mathrm{GeV}/c^2$. Plots (**a**, **b**) show the distribution of the transverse momentum p_{T} of the primary tracks before cut(6). Plots (**c**, **d**) give the invariant mass W_{00} of the primary track assuming a decay into two massless particles before cut(7). The *arrows* indicate the regions which are selected by the analysis

than $1\,\mathrm{GeV}/c$ which are expected from two-photon events are removed. After the cut, 89 data events were left, consistent with 88.3 events expected from standard model sources.

(7) The invariant mass W_{00} of the primary particle was calculated using the primary and secondary track momenta and assuming the hypothesis of a massive particle decaying into two massless particles (one visible, and one invisible). Low–mass resonances were rejected by requiring this mass to be greater than $4\,\mathrm{GeV}/c^2$. In Fig. 3b the distributions of the invariant mass for data and simulated background are shown. After the cut, 7 data events remained while 5.1 events are expected from standard model sources.

(8) Remaining background caused by shower electrons from Bhabha scattering which traverse the detector under small angles with respect to the beam axis were reduced by requiring that the angle between primary and secondary tracks be smaller than 172°. Also, a primary track having an angle smaller than 25° with respect to the beam axis must not point to a cluster in the electromagnetic calorimeter with an energy greater than 70% of the beam energy.

(9) Hadronic interactions were suppressed by rejecting a kinked track with more than two secondaries associated to its primary track. If there were two secondaries, the angle ζ between them was required to be smaller than 20° ($\cos\zeta < 0.93$) to keep sensitivity for decaying tau leptons.

After all cuts $1.83 \pm 0.42_{\mathrm{stat.}} \pm 0.47_{\mathrm{syst.}}$ events were expected background for the entire data set. The background consists of events with hadronic interactions of particles with the detector material, mainly from two-photon processes. No data event passed all the cuts, which is consistent with the expectation from standard model sources. Typical efficiencies of the selection for pair-produced smuons and staus are around 45%, independent of the sparticle mass. For selectrons the efficiency decreases to 25% at masses of $45\,\mathrm{GeV}/c^2$ as selectrons can be produced in the t-channel, which leads to a more forward production.

3.3.2 Event selection for neutralino pair-production

Searching for pair–produced neutralinos ($e^+e^- \to \tilde{\chi}_1^0\tilde{\chi}_1^0$, $\tilde{\chi}_1^0 \to \tilde{\tau}_1\tau$ or $\tilde{\chi}_1^0 \to \tilde{\ell}_{\mathrm{R}}\ell$) which decay into a lepton and the NLSP, the data were searched for topologies with a few tracks originating from the primary interaction point plus at least one kinked track. In the following list all cuts which are changed with respect to the search for pair-produced NLSPs (Sect. 3.3.1) are given.

(2*) The sum of the numbers of primary plus secondary tracks must be less than or equal to 25 and the number of good tracks should not exceed six.

(3*) There must not be more than four primary track candidates and to reject events from two-photon processes the scalar sum of their p_{T} has to be greater than $4\,\mathrm{GeV}/c$.

(7*) The invariant mass W_{00} of the primary particle has to be greater than $10\,\mathrm{GeV}/c^2$ to compensate for the relaxed cut on the number of tracks in the event.

As for all other selections of events with kinked tracks the remaining expected background of $1.05 \pm 0.35_{\mathrm{stat.}} \pm 0.50_{\mathrm{syst.}}$ events in this analysis consists of hadronic interactions from particles in two-photon events. One data event survived the complete selection which is consistent with the expectation. The efficiency for detecting neutralino pair-production followed by a delayed decay of the NLSP is typically around 40%, independent of the neutralino and NLSP mass.

3.3.3 Event selection for selectron and smuon pair-production (stau NLSP)

In the case of a cascade of pair-produced selectrons or smuons ($e^+e^- \to \tilde{\ell}_{\mathrm{R}}^+\tilde{\ell}_{\mathrm{R}}^-$, $\tilde{\ell}_{\mathrm{R}} \to \ell\tilde{\chi}_1^0$, $\tilde{\chi}_1^0 \to \tau\tilde{\tau}$) to a stau with its decay inside the tracking chamber, the events contain a few tracks originating from the primary vertex plus at least one kink vertex. The cut on the number of tracks in the event has to be relaxed compared to the search for directly produced NLSPs. This is compensated by a tighter requirement on the invariant mass W_{00} of the primary track. In the following list all cuts which are changed with respect to the search for direct NLSP production (Sect. 3.3.1) are given.

(2**) The sum of the numbers of primary plus secondary tracks must be less than or equal to 25 and the number of good tracks should not exceed ten.

(3**) There must not be more than eight primary track candidates, and to reject two-photon processes, the scalar sum of their transverse momenta p_{T} should be greater than $4\,\mathrm{GeV}/c$.

(7*) The invariant mass W_{00} of the primary particle has to be greater than $10\,\mathrm{GeV}/c^2$.

After all cuts $2.76 \pm 0.69_{\mathrm{stat.}} \pm 0.51_{\mathrm{syst.}}$ events are expected from standard model sources, mainly hadronic interactions with the detector material. Three events survived the selection in the entire data set, consistent with the expectation. One surviving candidate is the same as the one selected by the search for pair-produced neutralinos (Sect. 3.3.2). The efficiency to detect the production and decay of pair-produced selectrons and smuons in the stau NLSP scenario is around 30% for all slepton, neutralino and NLSP masses.

3.3.4 Statistical and systematic uncertainties

The expected standard model background for the kinked track search comes from hadronic interactions of particles with the detector material. All processes with charged particles in the final state can contribute to it. Because of a high production cross-section, of the order of 10 nb, for two-photon events the number of simulated events of this type is not much higher than the number of data events expected. Thus selecting such an individual event contributes significantly to the number of expected background events

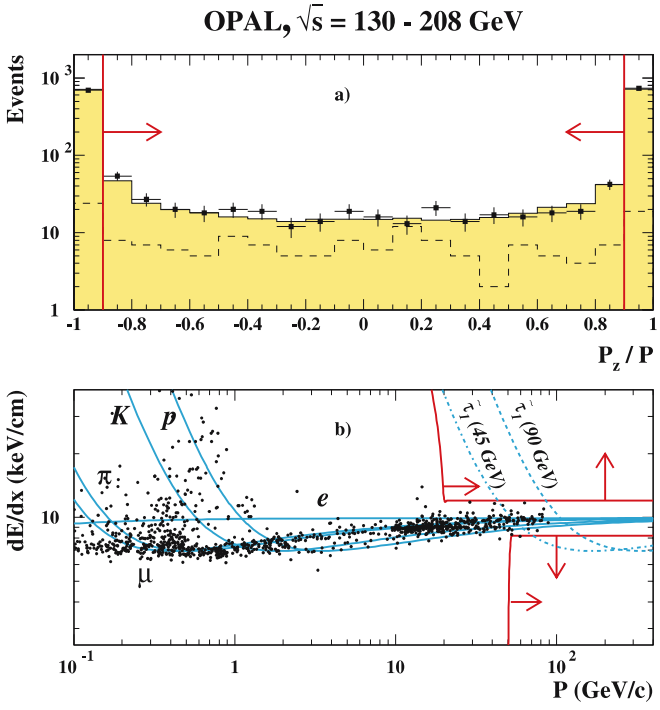

Fig. 4. Distributions of variables in the search for long-lived charged NLSPs before selection cuts. Plot **a** shows the scaled component P_z of the event momentum $P = |\mathbf{P}| = |\sum \mathbf{p}_{\mathrm{track}}|$ along the beam axis before cut(5), Sect. 3.4.2. The data, taken at centre-of-mass energies of 189–209 GeV are represented by *dots*, the simulated background from standard model sources by the *solid line*. The *dashed line* indicates the expected distribution for staus with a mass of $90 GeV/c^2$, pair-produced at a centre-of-mass energy of 208 GeV. In Plot **b** the distribution of candidate events before cut(9) as a function of the track momentum P and the specific ionization energy loss $\mathrm{d}E/\mathrm{d}x$ is given. In addition the expected energy loss for electrons (e), muons (μ), pions (π), kaons (K), protons (p) and long-lived staus ($\tilde{\tau}_1$ with $m_{\tilde{\tau}_1} = 45$ and $90 GeV/c^2$) is indicated. In both plots the *arrows* give the regions which are selected by the analysis cuts

and results in a significant statistical uncertainty, reaching up to 100% for a single centre-of-mass energy.

The selections of events with kinked tracks are mainly based on tracking information. Thus systematic uncertainties were estimated using the same method as the search for tracks with large impact parameters described in Sect. 3.2.4. The resolution of the parameters describing the tracks in the r–ϕ plane in the simulated background and signal samples was degraded by 10% and the resolution of the z parameters by 40%. The analyses were repeated on the smeared sample and differences with respect to the original results were counted as systematic uncertainties. For a single centre-of-mass energy, differences up to 100% were found.

3.4 Searches for long-lived charged NLSPs

If the slepton is the NLSP and the lifetime is such that the decay happens outside the detector volume the heavy charged particle has to traverse the central tracking detector. In this gaseous detector the measurement of the specific ionization energy loss $\mathrm{d}E/\mathrm{d}x$ along the particle's track allows a powerful identification of signal events.

3.4.1 Search for pair-produced stable charged NLSPs

The search for pair-produced long-lived massive particles with a lifetime longer than 10^{-7} s is reported in [8]. The search is used here to select candidate events for pair-produced charged NLSPs, $e^+e^- \to \tilde{\ell}_{\mathrm{R}}^+\tilde{\ell}_{\mathrm{R}}^-$. The selection is primarily based on the precise measurement of the ionization energy loss ($\mathrm{d}E/\mathrm{d}x$) of charged particles in the jet chamber, using a data set corresponding to a total integrated luminosity of 693.1 pb^{-1} between centre-of-mass energies of 130 and 209 GeV. No candidate event was reported in the entire data set which is consistent with the expectation from standard model background of 1.1 ± 1.3 events.

The typical efficiency of the search is about 95%; however, for particles with a $\beta\gamma = p/m = \sqrt{\frac{s}{4m^2} - 1}$ between 0.75 and 1.70, the efficiency drops below 5%. Figure 4 shows that this effect is due to the fact that in this particular $\beta\gamma$ region, the $\mathrm{d}E/\mathrm{d}x$ of tracks of heavy (SUSY) particles is very similar to that of light (standard model) particles. But since the LEP accelerator was operated at different centre-of-mass energies, particles with a certain mass were in different efficiency regions for different centre-of-mass energies.

3.4.2 Event selection for heavy stable charged particles in multi-track events

If long-lived NLSPs are produced as secondary or tertiary particles from the decays of neutralinos, charginos or heavier sleptons, their tracks are no longer back-to-back and additional tracks or additional missing energy are expected. The analysis searching for directly pair-produced NLSPs (Sect. 3.4.1) cannot be applied and a different analysis was developed to search for tracks with anomalous ionization energy loss in events with more than two tracks or additional missing energy. For all signal topologies one rather general data selection is chosen where at least one track per event with an anomalous specific energy loss is required.

The analysis was split into three steps:

1. preselection;
2. cuts on full event properties;
3. selection of high quality tracks with anomalous ionization energy loss.

(1) Preselection.

(P1) Events with either more than 20 tracks or with a low total visible energy less than $0.10\sqrt{s}$ were rejected to reduce the number of two-photon events.

(P2) There must be at least one track in the event which has at least one hit in the precision vertex chamber, 20 hits used for $\mathrm{d}E/\mathrm{d}x$ measurements and the specific energy loss should differ from that expected

from SM particles. For example, a track with momentum $p > 10\,\mathrm{GeV}/c$ must satisfy either $\mathrm{d}E/\mathrm{d}x > 11\,\mathrm{keV}/c\mathrm{m}$ or $\mathrm{d}E/\mathrm{d}x < 9\,\mathrm{keV}/c\mathrm{m}$.

(P3) Non-simulated backgrounds like cosmic muons and beam gas interactions are removed by requiring that the distance between the beam axis and the track at the point of closest approach had to be smaller than 1.5 cm in the x–y plane and smaller than 10 cm along the z coordinate. If there were hits in the time-of-flight barrel scintillators the measured time of the closest barrel hit was allowed to differ by at most 10 ns from the time expected from a physics event.

(2) Event Analysis.

(1) To reduce two–photon background events which deposit a large fraction of energy at small angles with respect to the beam axis, the maximum energy deposited in the forward calorimeters must be less than 5 GeV.

(2) The total measured relativistic invariant mass M_{vis} (visible mass) must satisfy $M_{\mathrm{vis}} > 10\,\mathrm{GeV}/c^2$ to reduce further the number of two–photon events.

(3) The total visible energy was required to satisfy $0.15 < E_{\mathrm{vis}}/\sqrt{s} < 1.10$, to reject two–photon and two–fermion events.

(4) The maximum electromagnetic cluster energy E_{ECAL} was required to satisfy $E_{\mathrm{ECAL}}/\sqrt{s} < 0.3$ to separate the signal from two–fermion processes.

(5) If the sum over all track momenta in an event $P = |\mathbf{P}| = |\sum \mathbf{p}_{\mathrm{track}}|$ was greater than $10\,\mathrm{GeV}/c$, the z component of the sum P_z must satisfy $|P_z/P| < 0.9$. This cut reduced mainly Bhabha scattering events with one electron escaping through the beam pipe carrying away a significant fraction of the total momentum of the event.

In the data set recorded between 189 GeV and 209 GeV, 572 data events survived the requirements on the event properties while 537.04 events are expected from standard model sources. Figure 4a shows the distribution of the variable $|P_z/P|$ used in cut (5) together with the distribution of an expected signal for pair-produced staus.

(3) Anomalous $\mathrm{d}E/\mathrm{d}x$ *selection.*

(6) In case the track with momentum p is associated to a cluster in the electromagnetic calorimeter with an energy E_{Cal}, the condition $E_{\mathrm{Cal}}/p \leq 0.15$ has to be satisfied. This cut further reduces Bhabha scattering events, four-fermion and two-photon background.

(7) To avoid events with converted photons – where the electron and positron tracks are unresolved by the tracking detectors, hence give a single track with a high $\mathrm{d}E/\mathrm{d}x$ – the track must have at least one hit in the high precision vertex chamber.

(8) The track had to satisfy tightened quality criteria. At least 40 hits should be used for $\mathrm{d}E/\mathrm{d}x$ measurement and the uncertainty on the momentum must be smaller than $10\,\mathrm{GeV}/c$.

(9) The track with momentum p must feature a high or low specific ionization energy loss $\mathrm{d}E/\mathrm{d}x$: if $p > a \cdot (\mathrm{d}E/\mathrm{d}x - b)$ then $\mathrm{d}E/\mathrm{d}x > 12.0\,\mathrm{keV}/c\mathrm{m}$ ($a = \frac{2}{17}\,\mathrm{cm}$, $b = 181.5\,\mathrm{keV}/c\mathrm{m}$) or if $p > 52\,\mathrm{GeV}/c$ then $\mathrm{d}E/\mathrm{d}x < 8.2\,\mathrm{keV}/c\mathrm{m}$ The cut separated signal topologies from standard model background.

(10) Finally, to separate the signal from standard model events with taus, no other track was allowed in a cone of 20° around the track with the anomalous $\mathrm{d}E/\mathrm{d}x$.

Figure 4b shows the distribution of the candidate events before cut (9) as a function of the track momentum and the specific ionization energy loss. The regions in which candidate events are expected are indicated. Out of 448 candidate events (419.33 events expected from Standard Model sources), no data event survived selection cut (9) while 0.89 events are expected.

The typical efficiency of the search ranges between 80% and 95% for masses of the heavy particle near the beam energy and between 20% and 40% for particles with a $\beta\gamma$ larger than 1.5. The efficiency drops below 5% only in a small region of $\beta\gamma$, where the ionization energy loss for massive particles is very similar to the energy loss of Standard Model particles, as shown in Fig. 4. In the data, recorded at $\sqrt{s} = 130$–$209\,\mathrm{GeV}$ and corresponding to an integrated luminosity of $\mathcal{L} = 632.1\,\mathrm{pb}^{-1}$, no event survived after all cuts. This is compatible with $0.78 \pm 0.38_{\mathrm{stat.}} \pm 0.10_{\mathrm{syst.}}$ events which are expected from the standard model sources.

Systematic uncertainties. The main tool used in this analysis is the information from particle tracks. Therefore, the main systematic uncertainties of the event selection arise from uncertainties in the track quality and the modeling of the specific energy loss in the simulation.

The systematic uncertainty arising from the track measurement was evaluated by smearing simulated track resolution by 5% for r–ϕ and 20% for z. Repeating the entire analysis with modified track parameters for signal and background determines the first contribution to the systematic uncertainty arising from the central tracking system. The second contribution to the systematic uncertainty is due to uncertainties in the modeling of the measured $\mathrm{d}E/\mathrm{d}x$ value. These uncertainties were evaluated by comparing muon pairs, Bhabha electrons, charged pions, and kaons in simulation and data, and found to be 10% of the measurement uncertainty $\sigma_{\mathrm{d}E/\mathrm{d}x}$. The contribution to the overall systematic uncertainty was determined by redoing the analysis of signal and background with the $\mathrm{d}E/\mathrm{d}x$ value of each track replaced by a value $(\mathrm{d}E/\mathrm{d}x \pm \sigma_{\mathrm{d}E/\mathrm{d}x})$.

The studies show that the number of expected background events may vary by 10% from the track smearing and by 5.0% due to the $\mathrm{d}E/\mathrm{d}x$ uncertainties.

4 Searches in the neutralino NLSP scenario

In this section the analyses to search for indirect NLSP production in the neutralino NLSP scenario are described. To be sensitive to all neutralino lifetimes, searches for

the production of sleptons and charginos were performed. Section 4.1 describes the analyses selecting event signatures expected for short-lived neutralinos with lifetimes up to 10^{-8} s. In Section 4.2 searches for neutralinos with a long lifetime are presented. A summary of the results for searches not described in other papers is listed in Table 3.

4.1 Searches for short-lived neutralinos

All signatures of SUSY particles in the scenario with the neutralino being the NLSP have in common that, for short and medium lifetimes up to 10^{-8} s, photons from the neutralino decay would be measured by the detector. For longer NLSP lifetimes, the decay happens outside the detector and typical signatures contain a significant amount of missing energy.

4.1.1 Search for events with photons and missing energy

The search for pair-produced neutralinos decaying in the detector volume selects events with two photons and large missing energy. The main background for the search is the standard model process $e^+e^- \to \nu\bar{\nu}$ + photons. The selection and the result of the search are described in [9]. No evidence is observed for new physics contributing to the expected final state.

4.1.2 Selection of events with isolated photons, missing energy, leptons and jets

If the lightest neutralino is the short-lived NLSP, the production and decay of scalar leptons ($e^+e^- \to \tilde{\ell}^+_{\rm R}\tilde{\ell}^-_{\rm R}$, $\tilde{\ell}^\pm_{\rm R} \to \ell\tilde{\chi}^0_1$) or charginos ($e^+e^- \to \tilde{\chi}^+_1\tilde{\chi}^-_1$, $\tilde{\chi}^\pm_1 \to W^\pm\tilde{\chi}^0_1$) lead to final states with missing energy, up to two photons plus leptons and/or jets ($\gamma(\gamma)\not{E}$ plus $q_i\bar{q}_j q_k\bar{q}_l$, $q_i\bar{q}_j\ell^\pm$ or $\ell^+\ell^-$). For each final state, the photon energy and the missing energy depend strongly on the mass difference $\Delta M (= M_{\rm NNLSP} - M_{\rm NLSP})$ between the pair-produced particle (the NNLSP) and the neutralino (the NLSP). Thus a set of analyses was designed, using a common preselection and followed by specific series of cuts optimized for the different ΔM regions:

(A) photons plus leptons and missing energy;
(B) photons plus jets and missing energy
  (B0) small ΔM ($< 20\,\mathrm{GeV}/c^2$),
  (B1) medium ΔM ($20 < \Delta M < M_{\rm NNLSP} - 30\,\mathrm{GeV}/c^2$),
  (B2) large ΔM ($> M_{\rm NNLSP} - 30\,\mathrm{GeV}/c^2$);
(C) photons plus jets plus a lepton and missing energy
  (C0) small ΔM ($< 20\,\mathrm{GeV}/c^2$) where analysis (B0) is used,
  (C1) medium ΔM ($20 < \Delta M < M_{\rm NNLSP} - 30\,\mathrm{GeV}/c^2$),
  (C2) large $\Delta M (> M_{\rm NNLSP} - 30\,\mathrm{GeV}/c^2)$.

The first part of the preselection required well-contained events from e^+e^- collisions and is identical to that used in the long-lived neutralino NLSP chargino search given in Sect. 4.2.2 and documented in [10]. The lepton and jet identification used here is also identical to that in [10]. All events with more than six good tracks from the interaction point and not originating from photon conversions were classified as candidates for selection (B) or (C), events with fewer tracks as candidates for selection (A).

The second part of the preselection picks up events with isolated photons and tightens the topological requirements.

(P1) There have to be at least two isolated photons with:
  – an electromagnetic cluster with an energy greater than 3 GeV;
  – the angle θ of the cluster with respect to the beam satisfying $|\cos\theta| < 0.9$;
  – in a 15° half-cone centred on the cluster the sum of track momenta and additional electromagnetic energies not exceeding 2 GeV.
(P2) The angle $\theta_{\rm miss}$ of the missing momentum had to satisfy $|\cos\theta_{\rm miss}| < 0.95$.
(P3) The transverse momentum of the event had to be greater than 3% of the centre-of-mass energy.
(P4) The visible energy in the event had to satisfy
  – $0.2 \cdot \sqrt{s} < E_{vis}/\sqrt{s} < 0.9 \cdot \sqrt{s}$ for analysis A,
  – $0.25 \cdot \sqrt{s} < E_{\rm vis}/\sqrt{s} < 0.85 \cdot \sqrt{s}$ for analysis B0 and
  – $0.4 \cdot \sqrt{s} < E_{\rm vis}/\sqrt{s} < 0.95 \cdot \sqrt{s}$ for the other analyses.
  In Fig. 5a the distribution of the visible energy in the event is shown for the data recorded at a centre-of-mass energy of 206 GeV together with the expected background. After cut (P4) of analysis A, 354 data events remained in the sample with 368.48 events expected in the background. Plot (b) shows the same distribution for a possible signal of stau pair-production at three different mass combinations of the stau and the neutralino.
(P5) The acoplanarity angle ϕ_{acop}, which is defined as the supplementary angle in a plane perpendicular to the beam direction between the two vectors which are obtained by summing up particle momenta after splitting the event into two jets using the Durham algorithm, has to satisfy $\phi_{acop} > 5°$.

After the preselection, the cuts were optimized depending on the mass difference between the NNLSP and the NLSP as well as the number of leptons expected in the event.

Selection (A): photons plus two leptons and missing energy. Events with two photons, two leptons and missing energy are expected from the production and decay of sleptons ($e^+e^- \to \tilde{\ell}^+_{\rm R}\tilde{\ell}^-_{\rm R}$, $\tilde{\ell}^\pm_{\rm R} \to \ell\tilde{\chi}^0_1$, $\tilde{\chi}^0_1 \to \gamma\tilde{G}$) and charginos ($e^+e^- \to \tilde{\chi}^+_1\tilde{\chi}^-_1$, $\tilde{\chi}^\pm_1 \to W^\pm\tilde{\chi}^0_1$, $\tilde{\chi}^0_1 \to \gamma\tilde{G}$) with both W bosons decaying leptonically. The main expected backgrounds from standard model sources are radiative return events to the Z boson, with $Z^0 \to \ell^+\ell^-$ accompanied by initial or final state radiation. To suppress this type of background, cuts on the photon energies are sufficient. The analysis does not distinguish between electrons, muons or taus since for small mass differences ΔM the lepton energy is small and they cannot be identified efficiently.

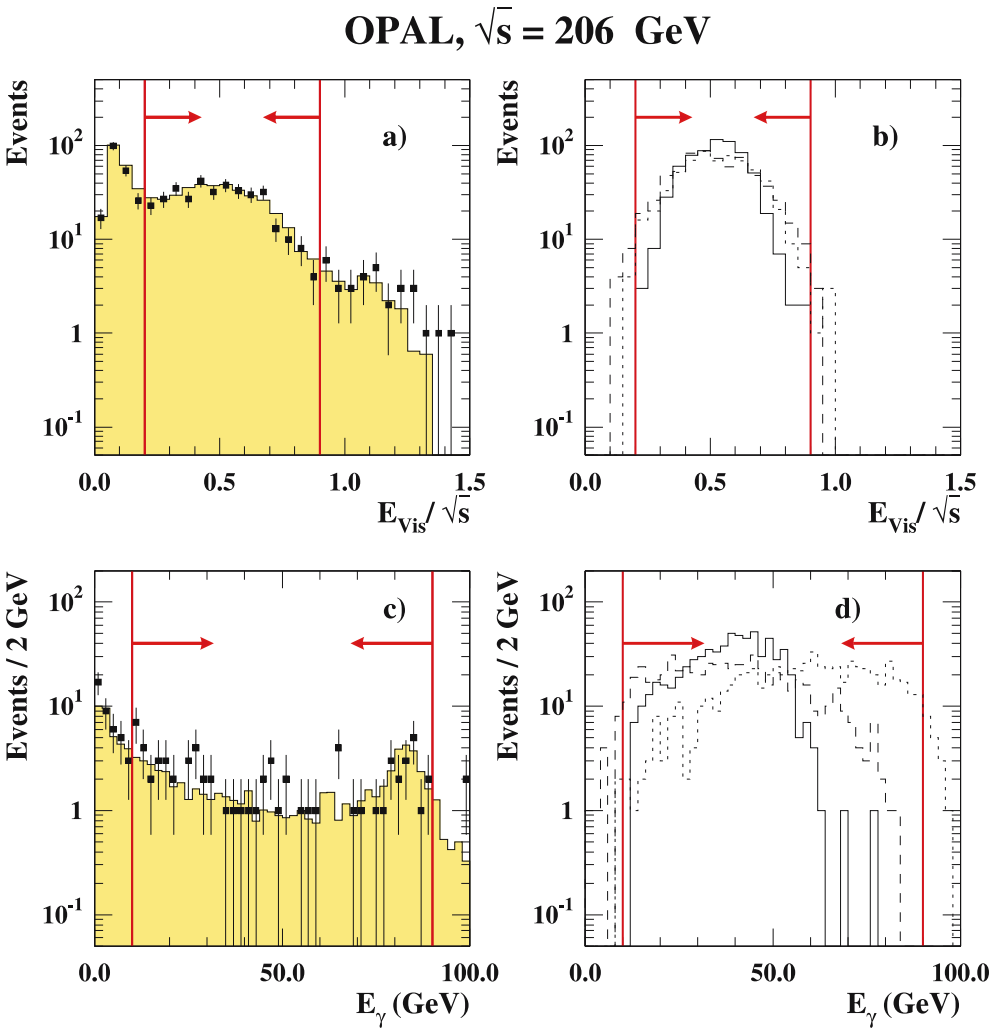

Fig. 5. Distributions of variables in the search for slepton and charginos with very short to medium lifetime Sect. 4.1.2, selection(A). Plots **a, b** show the distribution of the visible energy in the event as a fraction of the centre-of-mass energy, plots **c, d** the energies of the most energetic photon in the event. In **a** and **c** the data recorded at $\sqrt{s} = 206$ GeV are represented by *dots*, the expected standard model background by the *shaded histogram*. In **b** and **d** the distributions of a possible signal of stau pair-production in the neutralino NLSP scenarios are given. The *solid, dashed* and *dotted lines* correspond to $(\tilde{\tau}_1^{\pm}, \tilde{\chi}_1^0)$ mass combinations of (102, 51), (80, 20) and (50, 45) GeV/c^2. The *arrows* indicate the cut positions

(A-1) The energy E_γ of the most energetic photon had to be between 10 GeV and 90 GeV, and the energy of the second photon greater than 5 GeV. Almost all radiative return events were rejected by the requirement on the second most energetic photon. In Fig. 5c the energy distribution of the most energetic photon is shown for the data recorded at a centre-of-mass energy of 206 GeV together with the expected background. After the cut, 74 data events remained in the sample with 70.63 events expected in the background. Plot d shows the same distribution for a possible signal of stau pair-production at three different mass combinations of the stau and the neutralino.

(A-2) Surviving events with final state radiation often have the photon near a particle track. To reject them the transverse momentum of the photon with respect to the nearest track had to be larger than 10 GeV/c (5 GeV/c) for the first (second) photon.

In data recorded at centre-of-mass energies between 189 GeV and 209 GeV, 3 events survived the selection with $7.74 \pm 0.47_{\text{stat.}} \pm 1.63_{\text{syst.}}$ events expected from standard model sources.

Selection (B0): photons plus jets and missing energy for small ΔM. In the case of production and decay of charginos ($e^+e^- \to \tilde{\chi}_1^+\tilde{\chi}_1^-$, $\tilde{\chi}_1^{\pm} \to W^{\pm}\tilde{\chi}_1^0$, $\tilde{\chi}_1^0 \to \gamma\tilde{G}$) with both W bosons decaying into two jets for small mass differences between the chargino and the neutralino NLSP, the jets contain only a small amount of energy. The jets might not be measured well, thus the selection depends on the two most energetic photons only.

(B0-1) The energy of the most energetic photon has to be greater than 20 GeV and the energy of the second photon greater than 10 GeV.

(B0-2) The visible energy in the event, excluding the two most energetic photons, has to be less than 50 GeV.

After the selection there is no event left in the entire data set with $0.69 \pm 0.09_{\text{stat.}} \pm 0.14_{\text{syst.}}$ events expected from standard model sources.

Selection (B1): photons plus jets and missing energy for medium ΔM. In case of a higher mass difference between the chargino and the neutralino, the four jets of the hadronically decaying W bosons have significant energy,

and there is no prompt lepton in the events. The jets exclude the identified photons.

(B1-1) The number of identified, isolated leptons had to be zero. The lepton was defined to be isolated if there was not more than 2 GeV additional energy in a cone with a half-angle of 15° around the lepton.

(B1-2) To reject events with final state radiation, the transverse momentum of the photon with respect to the nearest track had to be larger than 10 GeV/c (5 GeV/c) for the first (second) photon.

Different additional requirements have to be fulfilled, depending on the number of jets in the event.

(B1-3) 4-jets: the angle between the two reconstructed W bosons had to be less than 150°, with the two bosons (jet pairs) being selected by minimizing the difference between the jet masses and the W boson mass $((M_{ij} - M_W)^2 + (M_{kl} - M_W)^2)$.
3-jets: the two jets with an invariant mass closest to the mass of the W boson were paired together. The angle between the W and the remaining jet had to be smaller than 150°.
2-jets: the sum of the opening angles between each jet and the most energetic photon had to be less than 356°.

After the selection 6 data events survived the cuts of the medium ΔM analysis (B1) with $8.59 \pm 0.86_{\text{stat.}} \pm 1.80_{\text{syst.}}$ events expected from standard model sources.

Selection (B2): photons plus jets and missing energy for large ΔM. Because of the large mass difference between the chargino and the neutralino, expected signal events have less energetic photons and only a small missing momentum. After the selection, the remaining backgrounds are mainly from the processes $e^+e^- \to W^+W^-$ and $e^+e^- \to Z^0\gamma$ with additional photons.

(B2-1) The number of identified, isolated leptons had to be zero.

(B2-2) To reject events with final state radiation, the transverse momentum of the photon with respect to the nearest track had to be larger than 5 GeV/c (3 GeV/c) for the first (second) photon.

(B2-3) The event was forced into four jets and the invariant mass cut of the Durham jet finding algorithm k_{T} had to satisfy $k_{\text{T}} > 4\,\text{GeV}/c^2$.

After the selection, 3 data events survived with $2.67 \pm 0.26_{\text{stat.}}$ events expected from standard model processes.

Selection (C1): photons plus jets plus one lepton and missing energy for medium ΔM. If one W boson decays into a lepton and a neutrino, the other hadronically, two photons, two jets and one lepton with lower energies are expected in the event. The lepton can be identified and candidate events had to satisfy the following constraints.

(C1-1) There had to be at least one isolated lepton in the event.

(C1-2) To reject events with final state radiation, the transverse momentum of the photon with respect to the nearest track had to be larger than 10 GeV/c (5 GeV/c) for the first (second) photon.

(C1-3) The lepton energy had to be less than 40 GeV and the invariant mass of the two jets less than 70 GeV/c^2. This reduced the background from $W^+W^- \to q\bar{q}\ell\nu$ where jets and lepton are more energetic compared to expected signal events.

One event survived the selection cuts for the medium ΔM analysis, with $0.62 \pm 0.11_{\text{stat.}} \pm 0.13_{\text{syst.}}$ events expected from standard model sources.

Selection (C2): photons plus jets plus one lepton and missing energy for large ΔM. In case of a large mass difference between the chargino and the neutralino the jets and lepton have more energy. The main expected background results from the decay of pair-produced W bosons, $W^+W^- \to \text{q}\bar{\text{q}}\ell\bar{\nu}_\ell$, with additional photon(s) from the initial and(or) final state radiation. The signal topology is similar to the standard model process, but it can be separated by requiring two isolated photons and unbalanced W bosons.

(C2-1) There had to be at least one isolated lepton in the event.

(C2-2) The transverse momentum of the photon with respect to the nearest track or jet had to be larger than 5 GeV/c (3 GeV/c) for the first (second) photon.

(C2-3) The angle between the two W bosons, where one W is reconstructed from the two jets and the other by the most energetic lepton and missing momentum, had to be less than 170°.

In the data sample, two events survived the selection cuts, with $2.94 \pm 0.31_{\text{stat.}}$ events expected from standard model processes.

Systematic uncertainties. The uncertainty associated with the photon isolation requirement is the dominant systematic uncertainty in these selections. It originates from the modeling of parton-level photon emission, jet fragmentation and detector simulation. Since it is difficult to estimate an uncertainty on each source, a total uncertainty is obtained inclusively by comparing data with Monte Carlo simulation using several cross-check samples. The studies are limited by the number of simulated events and a systematic uncertainty, which is at most 20%, is taken into account for all selections.

Uncertainty on the modeling of the other cut variables for simulated background and signal was also investigated. This was done by shifting the cut value within the possible uncertainty. This is negligible for signal events but not for the background, especially at large ΔM, because the topology is similar to standard model events and some cuts are set near to the peak of their distributions. Uncertainties from 3% for analyses (A) and (B0) up to 6% for the other analyses are reached.

4.2 Searches for long-lived neutralinos

In the case where the neutralino is the NLSP and has a lifetime longer than 10^{-7} s, it usually decays outside the detector volume. The topologies are similar to searches for supersymmetric particles in gravity-mediated SUSY breaking scenarios in which the stable neutralino is the lightest supersymmetric particle.

4.2.1 Search for di-lepton events with missing transverse momentum

If the pair-produced sleptons decay to a lepton and a long-lived neutralino, the signature of possible candidate events is two leptons with missing transverse momentum. The search for this type of events is reported in [7] and a short description can be found in Sect. 3.1.1.

The search for di-lepton events with missing transverse momentum is also sensitive to the pair-production of charginos. Here the chargino can decay either to a slepton and a neutrino, followed by the prompt decay of the slepton to a lepton and a long-lived neutralino, or the chargino can decay to a neutralino and a W boson with both W bosons decaying leptonically.

4.2.2 Search for charginos decaying into a neutralino and a W boson

Approximately $438\,\mathrm{pb}^{-1}$ of data recorded at centre-of-mass energies of 192–209 GeV were analyzed to search for evidence of chargino pair-production. No evidence for a signal was observed and the results of the search are reported in [10]. Search channels looking for charginos decaying into a neutralino and a W boson were used for the GMSB searches described in this paper. All decays of the W boson, the hadronic or leptonic decay, leading to topologies containing jets and missing energy, or jets with a lepton and missing energy were considered.

In case both W bosons decay leptonically, the results of the searches reported in [7], Sect. 4.2.1 were applied.

5 Analysis combination strategy

For all sparticle production and decay channels the results from several analyses at several centre-of-mass energies have to be combined. Although the different analyses are sensitive to distinct topologies, some correlation, an overlap between selected data, background and signal events, is expected. To treat the overlaps between the various analyses properly, all used the same signal Monte Carlo samples, which were generated for each search channel, as well as the same samples of the simulated standard model background. This allows, via an event-by-event comparison of the selected signal, expected background and selected data events, the determination of the overlaps between all combinations of the analyses used in each channel.

The selection efficiencies were split into exclusive selection efficiencies and overlap efficiencies: the efficiency for events selected by only one analysis are denoted as exclusive selection efficiencies; events that are selected by two or more analyses are described by overlap efficiencies. For example, for the case of three analyses, there are, in total, three exclusive selection efficiencies and four overlap efficiencies (three for the overlaps between each two analyses and one for the overlap among all three analyses).

For all search channels the signal efficiencies, i.e. exclusive selection efficiencies and significant overlap efficiencies, were determined at each generated mass–lifetime point of the signal Monte Carlo samples. For data as well as for the expected background events the overlaps between the different analyses were investigated. The overlap for the background was found to be negligible (< 0.01 events) in all slepton NLSP channels. No data event was selected by more than one analysis. The various overlap selections were treated as separate search channels when combining them with the exclusive selections in the limit calculations.

In order to avoid generating and processing excessive amounts of signal Monte Carlo samples and to achieve a good description of the efficiencies over the whole mass and lifetime range an interpolating function was determined to calculate the efficiencies at any given mass, lifetime point and centre-of-mass energy. This is particularly important in the case that the NLSP occurs at the end of a cascade decay. In this case, it is impossible to simulate all possible mass combinations of the SUSY particles, hence the efficiency of the analyses has to be determined by the kinematics of the NLSP. In the next section such a fit function is discussed.

5.1 The efficiency function

The general ansatz for the interpolating function uses the following assumptions:

- The decay of the NLSP is described by $\exp\left(-\frac{t}{\tau}\right)$, where t is the time since the NLSP production and τ is the NLSP lifetime.
- The detector to measure the decay is a sphere with a fiducial volume ranging from a radius l_{start} to a radius l_{stop}.
- The detection efficiency of the detector ϵ_{d} and the efficiency of the analysis ϵ_{a}, (overall efficiency $\epsilon_0 = \epsilon_{\mathrm{d}} \otimes \epsilon_{\mathrm{a}}$) are constant within the bounds l_{start} and l_{stop}.
- Initial and final state radiation are neglected, which is a good assumption for heavy particles near the kinematic limit.

The probability of detecting a particle is a function of its mean decay length l_{mean}, which is a function of its lifetime, τ, and its boost, $\beta\gamma$. For pair production, $\beta\gamma$ is a function of the particle mass, m_1, and centre-of-mass energy $\sqrt{s}$. Then the probability of an analysis with an overall efficiency ϵ_0 detecting a particle decay inside a detector with the radii l_{start} and l_{stop} is given by

$$\epsilon_{\mathrm{single}} = \epsilon_0 \left[\exp\left(-\frac{l_{\mathrm{start}}}{l_{\mathrm{mean}}}\right) - \exp\left(-\frac{l_{\mathrm{stop}}}{l_{\mathrm{mean}}}\right) \right] , \qquad (2)$$

with l_{mean}, the decay length of the particle, defined as

$$l_{\mathrm{mean}} = c\tau\beta_1\gamma_1 = c\tau\sqrt{\frac{s}{4m_1^2} - 1}\,. \qquad (3)$$

The values $\epsilon_{\mathrm{single}}$, l_{start} and l_{stop} are effective values which are determined by a fit of the efficiency function (2) to the efficiencies obtained for the signal Monte Carlo samples, treating each channel separately. Depending on whether an analysis accepts events where one or both pair-produced particles have to decay in the detector, the event selection efficiency $\epsilon_{\mathrm{event}}$ is given by

$$\epsilon_{\mathrm{event}} = 1 - [1 - \epsilon_{\mathrm{single}}]^2 \text{ or } \epsilon_{\mathrm{event}} = \epsilon_{\mathrm{single}}^2 \text{ respectively}\,.$$

These formulae are used to describe the selection efficiency of the search analysis as a function of the NLSP $\beta\gamma$ over a wide range of masses, lifetimes and production energies with three parameters, ϵ_0, l_{start} and l_{stop}. The input variables are the mass of the decaying particle, its lifetime and the centre-of-mass energy. For the calculation of the efficiency of the zero lifetime search, the parameter l_{start} can be set to zero as the sensitive volume starts at the interaction point. For the heavy charged stable particle search, the parameter l_{stop} can be set to infinity.

An example of the efficiencies described by the function is given in Fig. 6 for stau pair-production at $\sqrt{s} = 208$ GeV. Here the search for acoplanar leptons, for tracks with large impact parameters or kinks, the search for particles with anomalous specific ionization energy loss plus all overlap analyses are included.

5.1.1 The efficiency function for NLSP in cascade decays

If the particle T_1 with lifetime τ is not pair-produced but a decay product of another pair-produced particle T_0 with mass m_0 and energy $E_0 = \frac{\sqrt{s}}{2}$, the average decay length l_{mean} has to be replaced by

$$l_{\mathrm{mean}} = \beta_1\gamma_1 c\tau = \frac{|p_1|}{m_1} c\tau\,.$$

Here $|p_1|$, the average momentum of T_1, is calculated from the two-body decay of T_0 into T_1 and a second decay product.

5.1.2 Selection efficiency for long-lived, charged NLSP from cascade decays

The use of the average momentum in the calculation of the NLSP decay length l_{mean} as described in the previous section is only justified if the efficiency, as a function of the NLSP $\beta\gamma$, is a smooth function with moderate variation of the order of a few percent. As the efficiency of searches for long-lived, heavy particles from cascade decays drops drastically from about 80% to below 5% for a $\beta\gamma$ of the particle between 0.7 and 1.7, a different method has to be applied. Instead of using the average NLSP momentum $|p|/m$, the kinematically possible $\beta\gamma$ spectrum after the decay of a primary particle is used, following the ansatz

$$\epsilon = \int \epsilon_0(\beta_1\gamma_1, \beta_2\gamma_2) \cdot g(\beta_1\gamma_1, \beta_2\gamma_2)\,\mathrm{d}\beta_1\gamma_1\,\mathrm{d}\beta_2\gamma_2\,.$$

Here, ϵ_0 is the efficiency to select a signal event expressed as a function of the $\beta\gamma$ values of the two possible NLSPs. It is determined using simulated signal events. The normalized $\beta\gamma$ spectrum of the heavy stable charged particles is given by the function g. The spectrum is calculated assuming a flat energy spectrum of the stable particles in the kinematically accessible range and neglecting ISR.

5.1.3 Errors on the interpolated efficiencies

In addition to the systematic uncertainties on the selections described in the analysis sections, an additional source of the systematic uncertainty for the signal selection results from the interpolation of the efficiencies to different mass and lifetimes. Its size was estimated by recalculating the parameters of the efficiency function dropping the information of one simulated signal sample and comparing the interpolated efficiency with the achieved efficiency at this point. Deviations were found to be less than 3%. Finally the efficiency function was varied by the uncertainties on the fitted parameters ϵ_0, l_{start} and l_{stop}. Here an uncertainty of less than 1% was found. The total systematic uncertainty assigned to the efficiency function is calculated by adding the three terms in quadrature.

The efficiency function for long-lived, charged NLSPs in cascade decays, Sect. 5.1.2, has regions of rapid variation and an additional systematic uncertainty is assigned. In the region of NLSP $\beta\gamma$ between 0.75 and 1.70 the efficiency is varying rapidly to small values, and relative uncertainties up to 43% on the modelling and 31% on the interpolation of the function were found. In the high efficiency region, the two contributions were determined to be 11% on the modelling and 8% on the interpolation. These dominant effects were included in the calculation of the limits on the production cross-section of SUSY particles.

6 Constraints on particle production cross-sections

The absence of any significant excess of events in the data compared to the expected number of standard model events in any of the search analyses can be translated into limits on the production cross-section of the SUSY particles at the 95% confidence level. The limits were calculated using the program described in [31] which incorporates statistical and systematic uncertainties on the efficiency and the expected background as well as the uncertainties on the luminosity of the analyzed data samples and uncertainties on the expected cross-sections into the limits using numerical convolution. The version of the program used here has been extended to treat correlated systematic errors with a Monte Carlo technique, although the correlations have negligible effects for the results quoted in this

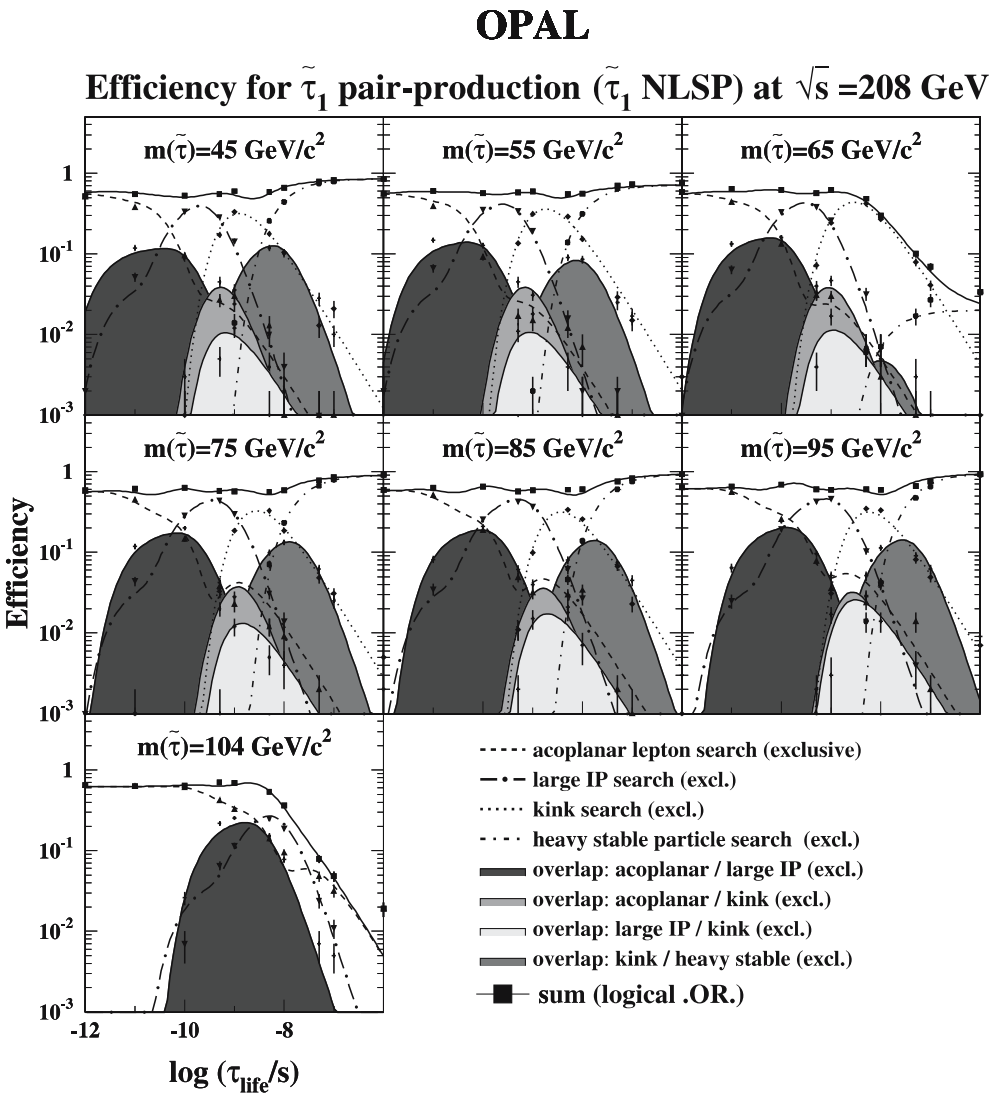

Fig. 6. Efficiencies for stau pair-production at $\sqrt{s} = 208$ GeV, as a function of the lifetime for fixed stau masses. The *symbols* represent the efficiencies for ten simulated lifetimes and the *curves* show the interpolating efficiency functions for the different searches: the exclusive search for promptly decaying staus (*dashed*), the exclusive search for large impact parameters (*long dashed-dotted*), the exclusive search for kinks (*dotted*) and the exclusive search for stable staus (*dashed-dotted*). The overlap efficiencies between these searches , if they exceed 0.1%, are shown as filled histograms. The sum of all efficiencies, i.e. the four exclusive selection efficiencies and the four overlap efficiencies, is shown by the *squares* and the corresponding *solid line*

paper. The results for each analysis were given at eight different bins of the centre-of-mass energy (see Table 3). For all analyses, systematic and statistical uncertainties on the signal efficiency and on the background expectation as well as uncertainties on the recorded luminosity were included.

Deriving cross-section limits at a single centre-of-mass energy requires knowledge of the cross-section evolution with $\sqrt{s}$ and, in general, this evolution depends on the details of the SUSY model. For direct NLSP pair-production, the GMSB model database described in Sect. 7 is scanned, and the cross-section evolution for each point in the database is used to calculate the cross-section limit at $\sqrt{s} = 208$ GeV for each mass and lifetime. The maximum excluded cross-section limit is chosen as the "model independent" limit for this mass and lifetime. For "lifetime independent" exclusions, the maximum cross-section limit valid for all lifetimes is chosen.

In the channels with cascade decays to the NLSP, this procedure does not work because there are points in the GMSB model with vanishing NNLSP production cross-sections and therefore the evolution is not defined. Instead, in these cascade channels, for spin 1/2 supersymmetric particles a β/s dependence of the cross-section is assumed, while for scalars a β^3/s dependence is used. The cross-section limits quoted in the cascade channels were evaluated for the "worst-case" of all intermediate particle masses, as well as NLSP lifetime.

6.1 The stau or slepton as the NLSP

Here the results of searches for signatures expected if the NLSP is the lightest slepton are described. The sleptons are either produced directly or appear as decay products of heavier pair-produced SUSY particles.

6.1.1 Cross-section limits for direct NLSP (stau or slepton) pair-production

To obtain constraints on the production cross-sections for slepton pair-production in the slepton co-NLSP scenario and stau pair-production in the stau NLSP scenario the search for acoplanar leptons (Sect. 3.1.1), the search for tracks with large impact parameters (Sect. 3.2.1), the

search for kinked tracks (Sect. 3.3.1) and the search for heavy stable charged particles (Sect. 3.4.1) were combined. A significant overlap of up to 40% in the signal efficiency was found between the acoplanar lepton and large impact parameter searches. The overlap between the acoplanar lepton and kink searches is about 4%, between the large impact parameter and kink searches about 7%, and between the kink and heavy stable charged particle searches up to 20%. Examples of the exclusive and overlap signal efficiencies can be seen in Fig. 6 for the stau searches. There is no data event selected in common, while for the expected background an overlap of 0.01 events was found between the large impact parameter and acoplanar lepton searches in the selectron and the stau channels.

The resulting limits at 95% C.L. at $\sqrt{s} = 208\,\text{GeV}$ are given in Fig. 7 for staus in the stau NLSP scenario (a) and for staus (b), smuons (c) and selectrons (d) in the slepton co-NLSP scenario. For all flavours the weakest exclusion is found in the very short lifetime region ($\tau = 10^{-12}$–10^{-11} s), due to the irreducible background from W^+W^- production in the acoplanar lepton topology, whereas all other regions are almost free of expected background. Also, the smaller sensitivity for masses around $60\,\text{GeV}/c^2$ at long lifetimes, due to the loss of sensitivity at $\mathrm{d}E/\mathrm{d}x$ band crossings as described in Sect. 3.4.1, is visible in all channels. Because of the highest selection efficiencies, the best constraints are obtained for smuons with an upper limit of 0.05 pb in most of the plane, apart from the region with a smuon mass above $100\,\text{GeV}/c^2$, close to the kinematic limit. For selectrons the constraints are slightly weaker. Here cross-sections larger than 0.1 pb can be excluded in most of the selectron mass–lifetime plane. The difference between smuons and selectrons is explained by the fact that selectrons can be produced in the t-channel, which leads to a more forward production and thus to lower efficiencies. For stau pair-production, cross-sections larger than 0.1 pb are excluded. The stau limits in the slepton co-NLSP scenario and in the stau NLSP scenario are rather similar, with a small difference due to the slightly different theoretical cross-sections that are used for the combination of the results at various centre-of-mass energies.

6.1.2 Cross-section limits for neutralino pair-production

Two scenarios exist in the theory: in the stau NLSP scenario the neutralino decays with 100% branching ratio to $\tilde{\tau}_1\tau$, while in the slepton co-NLSP scenario it decays with equal branching fractions to all flavours. Both cases were studied. Four analyses were combined: the search for events with four or more leptons plus missing energy

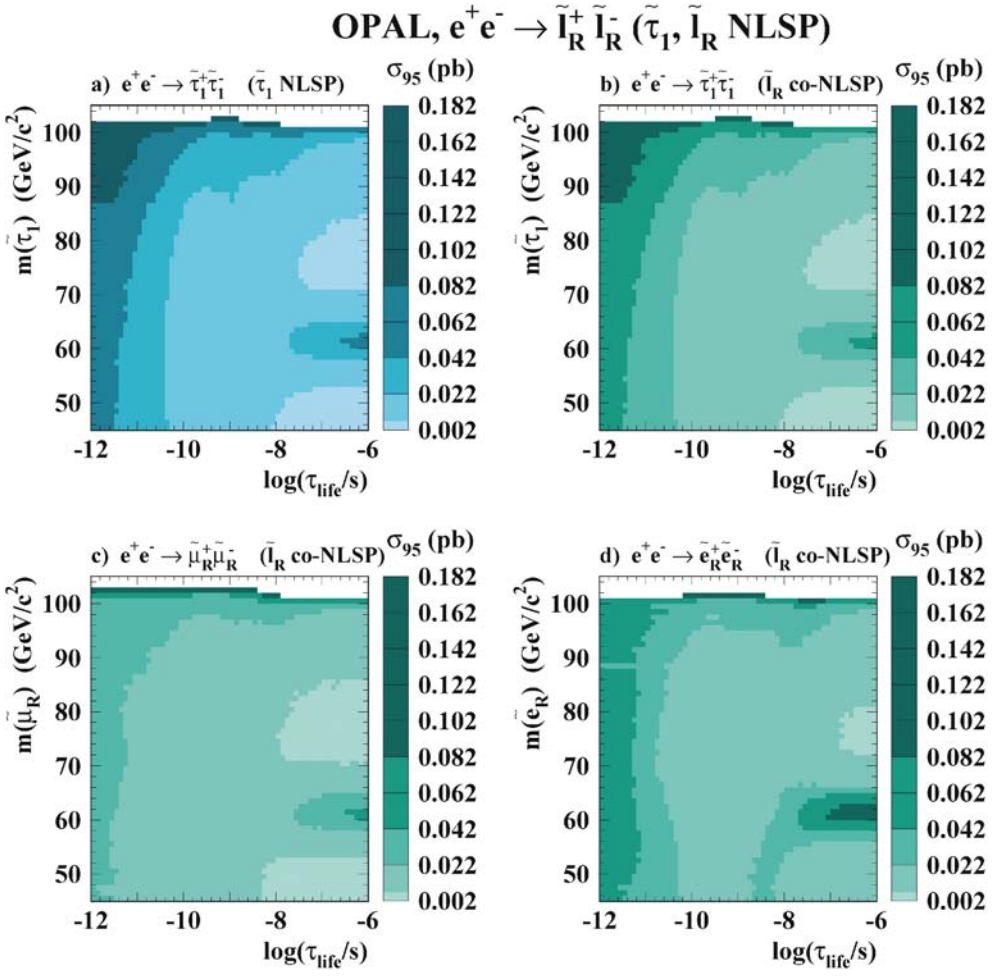

Fig. 7. Contours of the 95% C.L. upper limits on the production cross-sections σ_{95} for slepton pair-production at $\sqrt{s} = 208\,\text{GeV}$ as a function of the slepton mass and lifetime τ_{life}. Shown are cross-section limits for **a** staus in the stau NLSP scenario, **b** staus, **c** smuons and **d** selectrons in the slepton co-NLSP scenario. The shadings correspond to different ranges of the 95% C.L. upper limit on the cross-section, as indicated by the scale on the right side For the calculation of these limits four analyses were combined: the searches for acoplanar leptons, for large impact parameters, for kinks and for heavy stable charged particles

(Sect. 3.1.2), the searches for tracks with large impact parameters (Sect. 3.2.2) or kinks (Sect. 3.3.2) and the search for tracks with an anomalous ionization energy loss in events with more than two tracks (Sect. 3.4.2). No indication of new physics was observed in any of the analyses. Significant overlaps exist in the signal efficiency between the search for four leptons plus missing energy and the large impact parameter search (up to 20%) and between the large impact parameter and the kinked track search (up to 15%). The efficiencies in the overlap of other selections were found to be less than 0.1%. No data event was selected in common by two analyses. This is compatible with the shared expected background of 0.01 events between the search for multi-leptons plus missing energy and the large impact parameter search and no expected event for the other combinations. The results of the different analyses were combined assuming a β/s dependence of the production cross-sections at the various centre-of-mass energies.

Limits on the production cross-section of neutralino pairs at $\sqrt{s} = 208\,\text{GeV}$ in the stau NLSP case are shown in Fig. 8. In a the limit valid for all NLSP lifetimes is given. In most regions, cross-sections larger than 0.1 pb can be excluded, except for low mass differences between the neutralino and the stau. Figure 8b shows the NLSP lifetimes at which the maximum cross-section limit is reached. For small mass differences between the neutralino and the stau, the limit is set by the short lifetime searches, whereas the searches for intermediate lifetimes set the limit in the rest of the parameter space. Figure 8c shows the excluded cross-section for a short-lived NLSP and cross-sections larger than 0.1 pb can be excluded. Figure 8d shows the exclusions of values larger than 0.05 pb for a long-lived NLSP.

In the slepton co-NLSP scenario, slightly better results are obtained because of higher efficiencies of the short lifetime analyses for muons and electrons compared to tau searches. As shown in Fig. 9a, cross-sections larger than 0.1 pb can be excluded for all NLSP lifetimes, even for small mass differences between the neutralino and the slepton. Figure 9b illustrates that the limits are set by the medium lifetime searches in most cases, while for small mass differences they are set by the short lifetime searches. Figures 9c and d give the excluded cross-sections for a short-lived NLSP and a long-lived NLSP, with typical excluded cross-sections larger than 0.1 pb and 0.05 pb, respectively.

6.1.3 Cross-section limits for smuon and selectron pair-production (stau NLSP)

To search for pair-produced selectrons and smuons which decay via a (virtual) neutralino to the stau, the NLSP, four

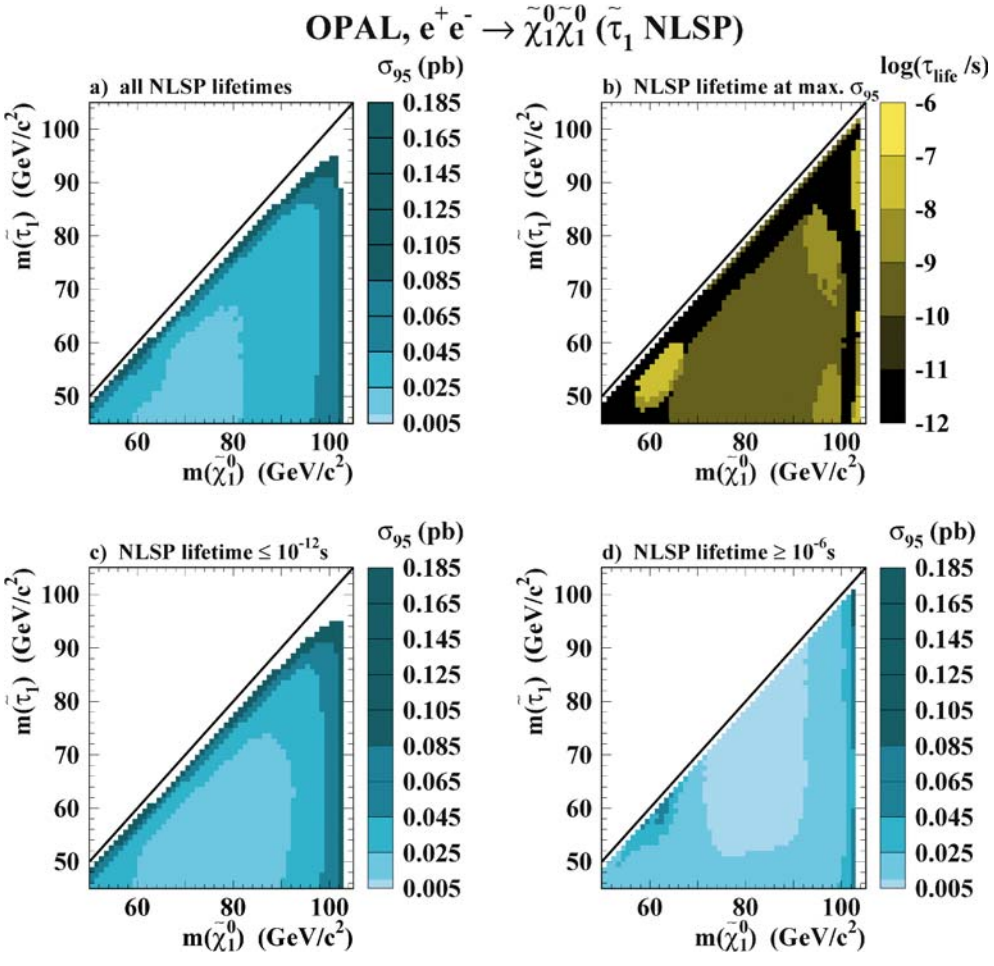

Fig. 8. Upper limits at 95% C.L. on the production cross-section for neutralino pairs in the stau NLSP scenario at $\sqrt{s} = 208$ GeV. The data analyzed, taken at different centre-of-mass energies, were combined assuming a β/s dependence of the cross-sections. In **a** the lifetime independent exclusions are shown as a function of the neutralino and NLSP mass. The lifetime at which the limit is set is given in **b**. Figures **c** and **d** give the excluded production cross-section for neutralinos assuming a very short-lived or a stable NLSP

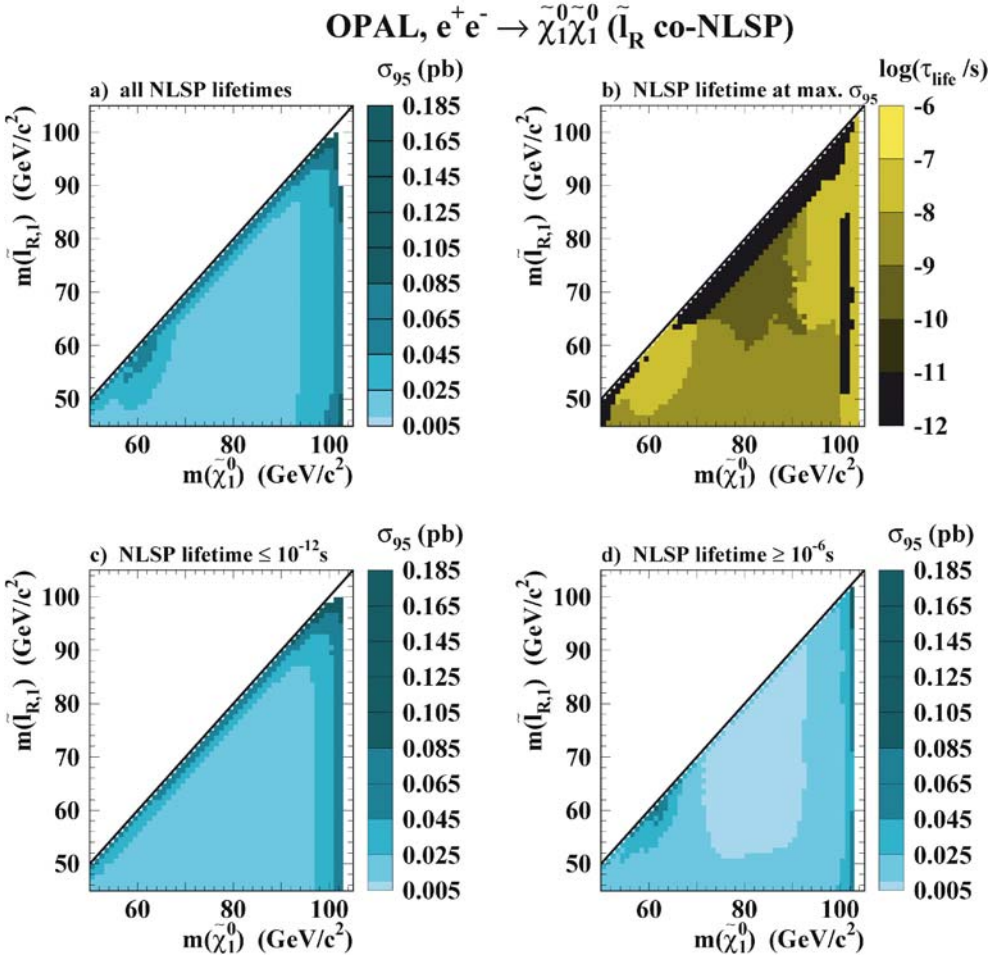

Fig. 9. Upper limits at 95% C.L. on the production cross-section for neutralino pairs in the slepton co-NLSP scenario at $\sqrt{s} = 208$ GeV. The data analyzed, taken at different centre-of-mass energies, were combined assuming a β/s dependence of the cross-sections. In **a** the lifetime independent exclusions are shown as a function of the neutralino and NLSP mass. The lifetime at which the limit is set is given in **b**. Figures **c** and **d** give the excluded production cross-section for neutralinos assuming a very short-lived or a stable NLSP

searches were combined. Topologies with a promptly decaying NLSP were searched for using the analysis sensitive to four or more leptons plus missing energy (Sect. 3.1.2). Candidate events for NLSPs with a medium lifetime were identified with the large impact parameter (Sect. 3.2.3) or kink search (Sect. 3.3.3), while possible stable NLSPs were searched for by selecting tracks with an anomalous ionization energy loss in events with more than two tracks (Sect. 3.4.2). For all four analyses, the number of selected data events is compatible with the number expected from standard model sources.

Significant overlaps for the signal efficiency exist between the search for multi-leptons plus missing energy and the large impact parameter search (up to 26%), between the multi-lepton search and the kink search (up to 10%) and between the large impact parameter and the kink search (up to 7%). For the expected background, an overlap of 0.01 events was found between the search for multi-leptons plus missing energy and the large impact parameter search. In the overlap regions of other analyses no event is expected to be selected in common.

The results for the different analyses were combined assuming a β^3/s dependence of the production cross-sections at the various centre-of-mass energies. Figure 10a shows the upper limit at 95% C.L. on the production cross-section of smuon pairs as a function of the NLSP mass at $\sqrt{s} = 208$ GeV for any lifetime of the NLSP. Cross-sections larger than 0.4 pb can be excluded, independent of the neutralino and NLSP mass, except for low mass differences between the smuon and the stau. The limit is set at short NLSP lifetimes in most cases, while for smuon masses below 65 GeV/c^2 the maximum excluded cross section is given by searches for a stable NLSP (Fig. 10b). Figure 10c shows that for a short-lived NLSP cross-sections larger than 0.4 pb can be excluded. For a long-lived NLSP limits on the production cross-section of smuon pairs less than 0.1 pb are achieved (Fig. 10d).

Similar values of the excluded production cross-section are achieved for selectrons as shown in Fig. 11.

6.1.4 Cross-section limits for chargino pair-production

In the scenarios with a stau or a slepton being the NLSP, the charginos decay to the NLSP plus a neutrino. Thus the signature visible in the detector is similar to the one expected from direct slepton NLSP pair-production except for an additional significant amount of missing energy which is taken away by the neutrino. If the NLSP decays promptly or inside the detector volume the same searches as for direct NLSP production can be applied. These are the searches for acoplanar leptons (Sect. 3.1.1), for tracks with large impact parameters (Sect. 3.2.1) and for kinked

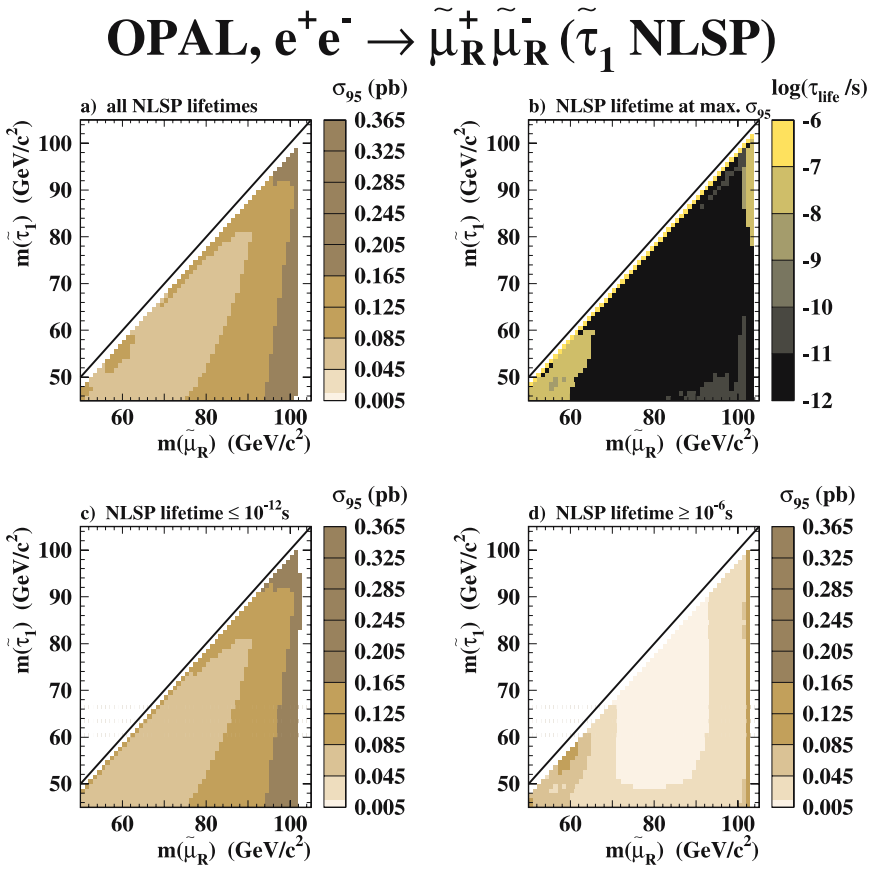

Fig. 10. Upper limits at 95% C.L. on the production cross-section for smuon pairs in the stau NLSP scenario at $\sqrt{s} = 208$ GeV. The data analyzed, taken at centre-of-mass energies of $\sqrt{s} = 189$–209 GeV, were combined assuming a β^3/s dependence of the cross-section. In **a** the lifetime independent exclusions are shown as a function of the smuon and NLSP mass. The lifetime at which the limit is set is given in **b**. Figures **c** and **d** give the excluded production cross-section for smuons assuming a very short-lived or a stable NLSP

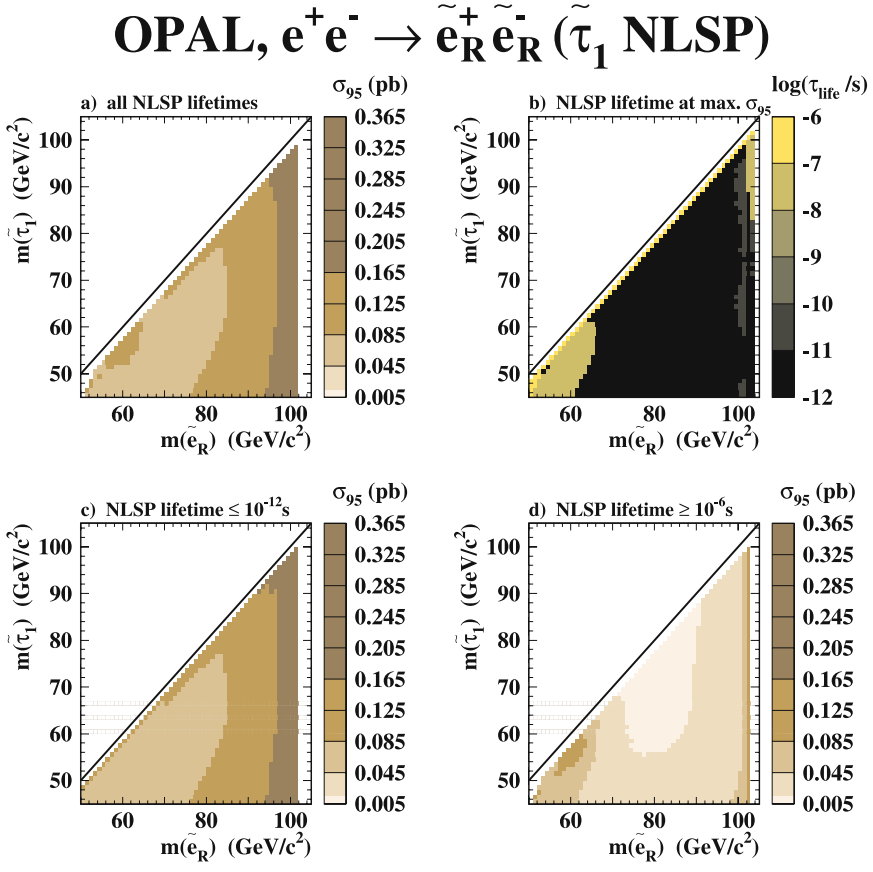

Fig. 11. Upper limits at 95% C.L. on the production cross-section for selectron pairs in the stau NLSP scenario at $\sqrt{s} = 208$ GeV. The data analyzed, taken at centre-of-mass energies of $\sqrt{s} = 189$–209 GeV, were combined assuming a β^3/s dependence of the cross-section. In **a** the lifetime independent exclusions are shown as a function of the selectron and NLSP mass. The lifetime at which the limit is set is given in **b**. Figures **c** and **d** give the excluded production cross-section for selectrons assuming a very short-lived or a stable NLSP

tracks (Sect. 3.3.1). In case of a long-lived NLSP the analysis described in Sect. 3.4.2 has to be applied as the two NLSP tracks are no longer back-to-back. No sign of new physics was observed by any of the four searches nor their overlap analyses.

For the exclusive and overlap analyses, the efficiency functions for NLSP pair-production with a stau or slepton NLSP were used, taking into account that the NLSP is a secondary particle. Thus, the efficiency function uses the average $\beta\gamma$ of the NLSP which is calculated from the kinematics of a two-body chargino decay, as described in Sect. 5.1.1. It was checked using a full simulation of chargino events that the applied interpolating functions describe the efficiencies well.

Cross-section limits were calculated both for the case of equal branching ratios of the chargino to all NLSP flavours in the slepton co-NLSP scenario and 100% branching ratio to the stau in the stau NLSP scenario. The data recorded at various centre-of-mass energies were combined assuming a β/s dependence of the cross-sections.

Figure 12a shows the upper limit at 95% C.L. on the production cross-section of chargino pairs at $\sqrt{s} = 208$ GeV for any lifetime of the stau NLSP. Cross-sections larger than 0.2 pb can be excluded for all chargino masses, independent of the NLSP mass. The limit is set at short NLSP lifetimes, except for chargino masses below 65 GeV/c^2 or close to the kinematic limit where the maximum excluded cross section is given by searches for a stable NLSP (Fig. 12b). Figure 12c shows that for a short-lived NLSP cross-sections larger than 0.2 pb can be excluded. For a long-lived NLSP limits on the production cross-section of chargino pairs less than 0.1 pb are achieved (Fig. 12d).

Similar values of the excluded production cross-sections are found for charginos in the slepton co-NLSP scenario as shown in Fig. 13.

6.2 The neutralino as the NLSP

6.2.1 Cross-section limits for neutralino pair-production

Directly produced NLSP pairs are searched for by the acoplanar photon search, which is sensitive to NLSP decay lengths of about 10 cm, corresponding to a lifetime of 10^{-9} s. If one or both neutralinos decay outside the detector, there is no acceptance by any analysis.

Figure 14 gives the excluded production cross-section for neutralino pairs at a centre-of-mass energy of $\sqrt{s} =$ 208 GeV. Cross-sections larger than 0.04 pb can be excluded for masses of the short-lived neutralino ranging from 45 GeV/c^2 up to the kinematic limit.

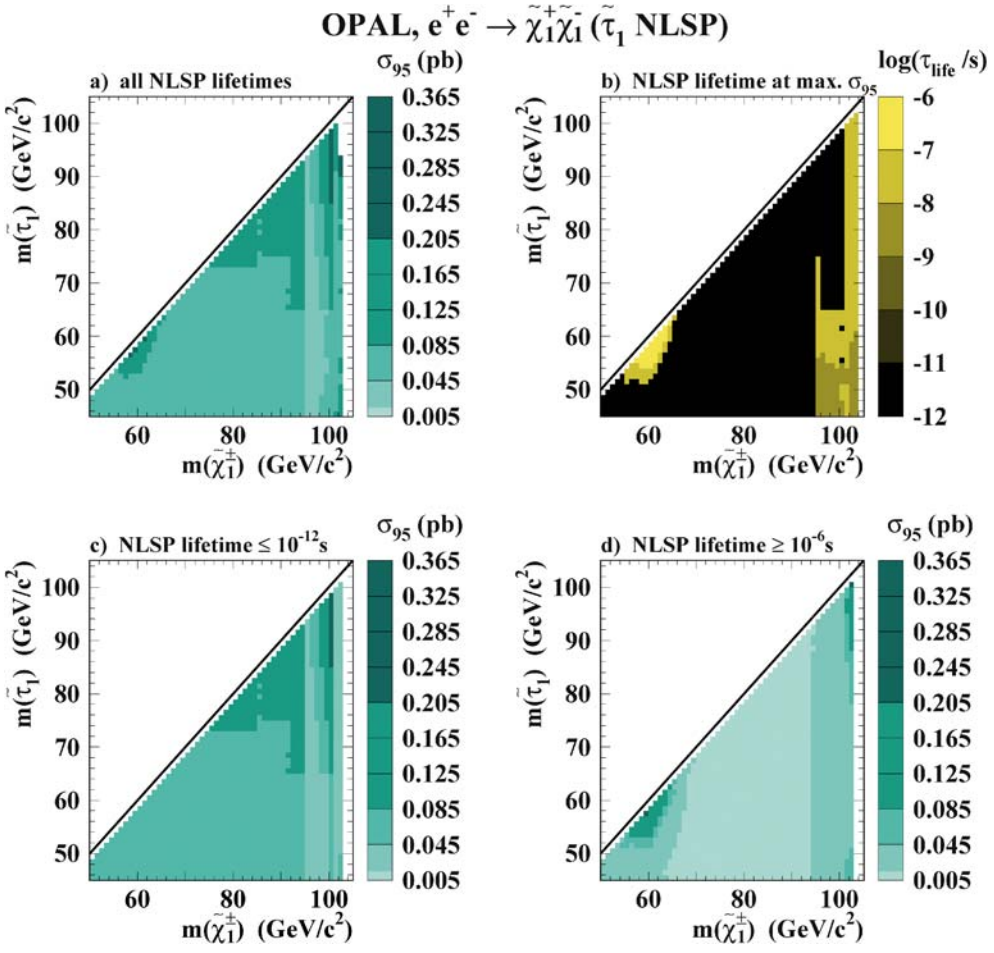

Fig. 12. Upper limits at 95% C.L. on the production cross-section for chargino pairs in the stau NLSP scenario at $\sqrt{s} =$ 208 GeV. The data analyzed, taken at different centre-of-mass energies, were combined assuming a β/s dependence of the cross-sections. In **a** the lifetime independent exclusions are shown as a function of the chargino and the NLSP mass. The lifetime at which the limit is set is given in **b**. Figures **c** and **d** give the excluded production cross-section for charginos assuming a very short-lived or a stable stau

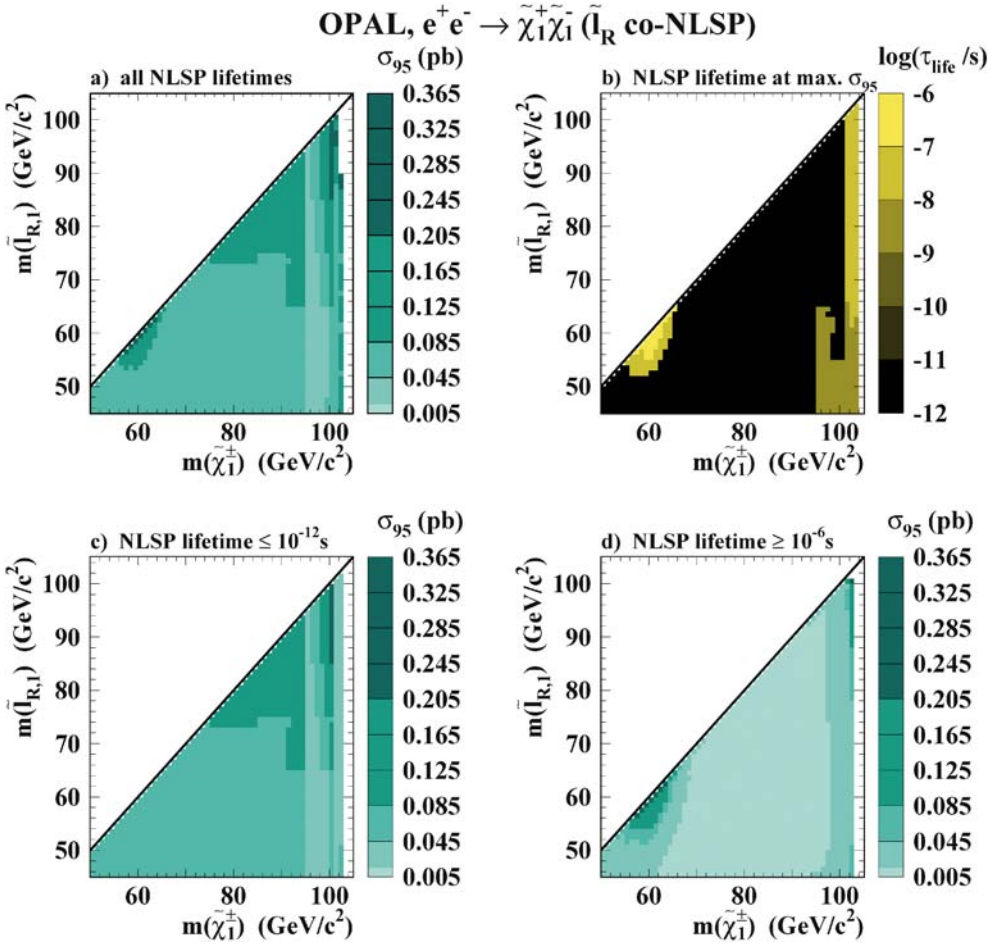

Fig. 13. Upper limits at 95% C.L. on the production cross-section for chargino pairs in the slepton co-NLSP scenario at $\sqrt{s} = 208$ GeV. The data analyzed, taken at different centre-of-mass energies, were combined assuming a β/s dependence of the cross-sections. In **a** the lifetime independent exclusions are shown as a function of the chargino and the NLSP mass. The lifetime at which the limit is set is given in **b**. Figures **c** and **d** give the excluded production cross-section for charginos assuming a very short-lived or a stable NLSP

6.2.2 Cross-section limits for slepton pair-production

To search for pair-produced sleptons in the neutralino NLSP scenario, two analyses were applied. For short NLSP lifetimes with a decay length of the neutralino up to 3 m ($\tau \leq 10^{-8}$ s) the search for leptons plus photons and missing energy (Sect. 4.1.2) has sensitivity. Long NLSP lifetimes ($\tau \geq 10^{-8}$ s) were covered by the search for acoplanar leptons (Sect. 3.1.1). For each flavour of the slepton an optimized analysis was used. The overlap of efficiencies between the analyses is of the order of 15% and a standard model background of less than 0.01 events is expected for the overlap analyses. For all searches the results from the data recorded at centre-of-mass energies of 189 GeV to 209 GeV were used. No indication for new physics in addition to the expected standard model background was observed. The datasets at different centre-of-mass energies were combined assuming a β^3/s dependence of the cross-sections.

Figures 15, 16 and 17 show the production cross-sections excluded at 95% C.L. for selectrons, smuons and staus, respectively. Plot (a) of each figure gives the excluded cross-section valid for any NLSP lifetime as a function of the slepton and the neutralino masses. Values larger than 0.2 pb can be excluded for all slepton flavours, independent of the neutralino mass. In plot (b) of each figure it is shown that the limit is set at NLSP lifetimes where the cross-over of the efficiencies of the two analyses takes place, shifting toward higher lifetimes with higher NLSP masses. Plots (c) and (d) of each figure give the excluded production cross-sections assuming a short-lived or long-lived NLSP. For both lifetime cases and for all flavours cross-sections higher than 0.1 pb can be excluded.

6.2.3 Cross-section limits for chargino pair-production

To be sensitive to all possible signatures for pair-produced charginos in the neutralino NLSP scenario, a large set of analyses had to be combined. For short NLSP lifetimes, the search for photons and missing energy plus leptons or jets is applied (Sect. 4.1.2), which is split into several selections, optimized for low and high track multiplicities in the event. The high multiplicity selection itself is divided into three parts, optimized for different mass differences between the chargino and the NLSP. Long lifetime neutralinos in chargino candidate events are selected by the search for acoplanar leptons in case of leptonically decaying W bosons. For semi-leptonic and hadronic W decays the chargino/neutralino searches with and without an identified lepton were applied.

For the acoplanar lepton search and for the search for photons and missing energy plus leptons or jets data at centre-of-mass energies $\sqrt{s} = 189$–209 GeV were analyzed. For the chargino searches with a semi-leptonic and hadronic W decay and a long-lived neutralino, data

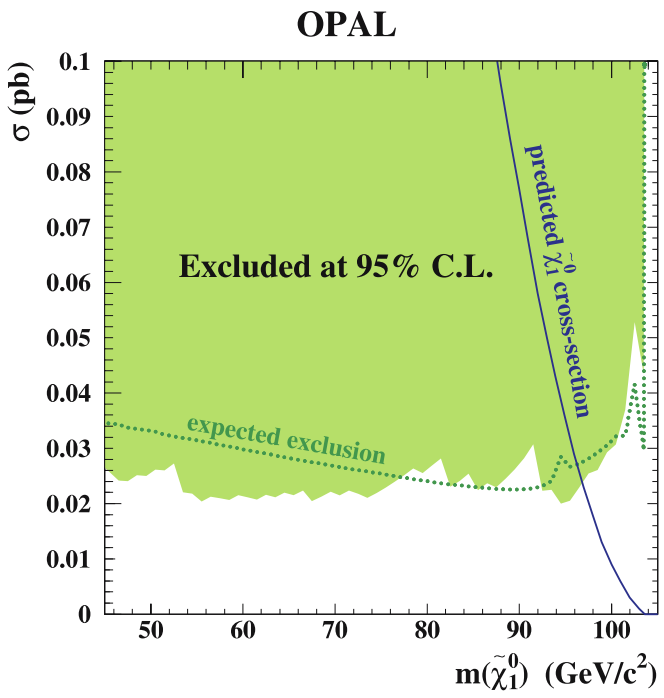

Fig. 14. The excluded production cross-section at $\sqrt{s} = 208$ GeV for neutralino pairs in the neutralino NLSP case is given by the grey region. The *dotted line* represents the expected limit. Both limits are given at 95% C.L. The *solid line* shows the minimum cross-section for neutralino pairs predicted by the theory. Within the model, neutralino masses between 45 GeV/c^2 and 96.8 GeV/c^2 (96.3 GeV/c^2 expected) can be excluded. The result is valid for promptly decaying NLSPs only

at $\sqrt{s} = 192$–209 GeV were used. No indication for new physics was found for any of the analyses. Limits on the production cross-section for charginos were computed, with the results at different centre-of-mass energies combined assuming a β/s dependence of the cross-sections and a pure decay of the chargino via a W boson.

Figure 18 gives the excluded production cross-section at 95% C.L. and for $\sqrt{s} = 208$ GeV for chargino pairs. The limits in (a) are valid for all NLSP lifetimes; cross-sections larger than 0.3 pb can be excluded for most chargino and NLSP masses. As can be seen in (b), this limit is set at NLSP lifetimes where the cross-over of the sensitivity of the lifetime analyses takes place, shifting toward higher lifetimes with higher NLSP mass (lower $\beta\gamma$ of the NLSP). Figures (c) and (d) give the excluded production cross-section assuming a short-lived or long-lived NLSP. For short-lived NLSPs, cross-sections higher than 0.2 pb, for long-lived NLSPs, cross-sections higher than 0.3 pb can be excluded.

7 Interpretations in the framework of the GMSB model

7.1 The GMSB scan database

Interpreting the experimental results in terms of the GMSB model requires a comparison with the theoretical expectations within the framework of the model. Chosen here is the minimal version of the GMSB model with five parameters and a sign in addition to the SM parameters. The new parameters are the SUSY breaking scale, $\sqrt{F}$, the messenger scale, M, the messenger index, N, the ratio of the vacuum expectation values of the two Higgs doublets, $\tan\beta$, the sign of the Higgs sector mixing parameter, sign(μ), and the mass scale Λ, which determines the SUSY particle masses at the messenger scale. A certain point in the parameter space of the model is excluded if the experimental upper limit on the cross-section at $\sqrt{s} = 208$ GeV discussed in Sect. 6 is less than the expected cross-section σ at $\sqrt{s} = 208$ GeV, taking into account the branching ratio BR ($\sigma \times \mathrm{BR}^2$ for pair-produced particles decaying to the same final state).

The parameter of the SUSY breaking scale $\sqrt{F}$ is eliminated as experimental upper limits were calculated on the production cross-section of SUSY particles independent of the NLSP lifetime (1). In the phase space of the remaining parameters a scan was performed to calculate the complete mass spectrum, production cross-sections and branching ratios for different SUSY particles at each point considered. For this scan the framework and formulae of [4] were used and generalized to include a full mass treatment for all three generations. The calculations are embedded in the SUSYGEN generator.

The model parameters as well as the range and step size considered for them are summarized in Table 4. The messenger scale M is arbitrary in the minimal model, but, as the mass m_b of the messenger bosons is given by $m_\mathrm{b} = M\sqrt{1 \pm \Lambda/M}$, the relation $M > \Lambda$ has to be fulfilled in order to obtain a positive messenger boson mass squared. Both models with $M \sim \Lambda$ and $M \gg \Lambda$ are viable; therefore, three scenarios for the messenger scale were studied: M very close to Λ ($M = 1.01 \cdot \Lambda$), $M = 250$ TeV/c^2 and M very large (10^6 TeV/c^2). For the integer parameter N, values up to five were considered. This is adequate, since perturbativity of the gauge interactions up to the grand unification scale, M_GUT, implies $N \lesssim 150/\ln\frac{M_\mathrm{GUT}}{M}$ [2]. Thus, for a messenger mass scale $M = 100$ TeV/c^2, $N \leq 5$ is required. Both signs of the parameter μ were considered. For each of the 30 combinations of N, M and sign(μ), a scan was performed in Λ and $\tan\beta$. The upper and lower limits for this scan were chosen according to the following considerations. For $\Lambda > 150$ TeV/c^2 the supersymmetric particles are already very heavy and cannot be produced at LEP energies. Both the regions with $\tan\beta > 50.0$ and $\Lambda < 5$ TeV/c^2 are theoretically forbidden. The exact shape of the theoretically inaccessible region in the $\Lambda - \tan\beta$ plane depends on the other parameters.

The scan information was saved in a database for comparison with the experimental results. In total, 270 such data sets were produced: 30 (with different N, M and sign(μ)) for each centre-of-mass energy and for nine different energy points with $\sqrt{s} = 182.7$, 188.7, 191.6, 195.5, 199.5, 201.6, 205.1, 206.7 and 208.1 GeV.

A gravitino mass of 2 eV/c^2 was chosen, corresponding to a SUSY breaking scale of $\sqrt{F} \approx 100$ TeV/c^2. This

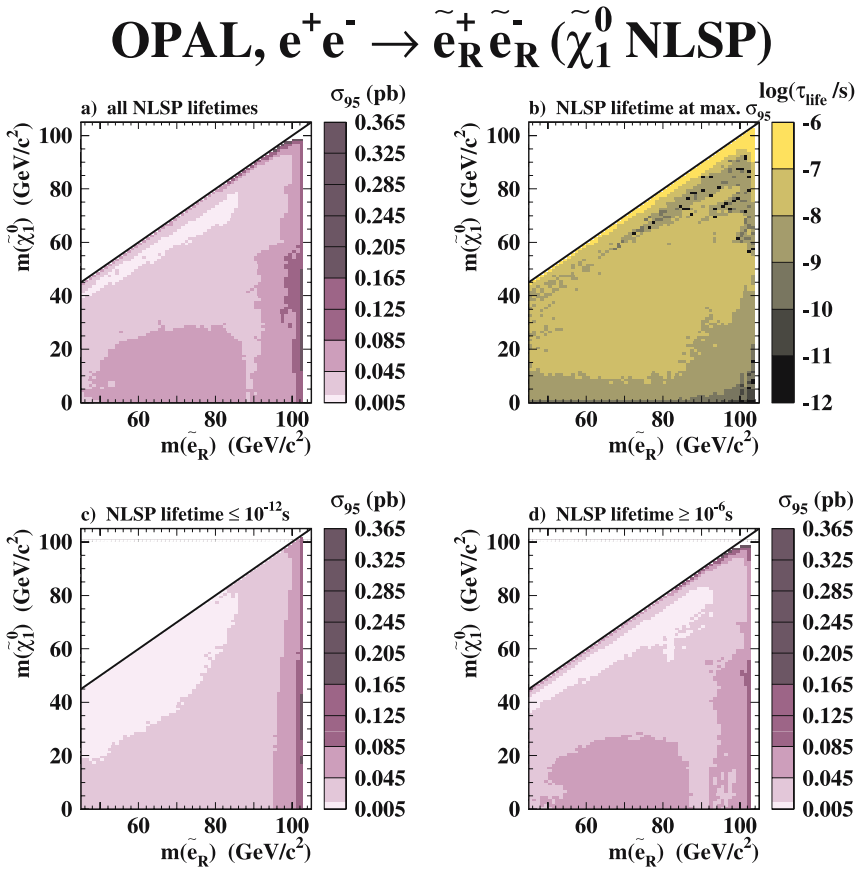

Fig. 15. Contours of the cross-section limits at 95% C.L. and $\sqrt{s} = 208$ GeV for selectron pair-production in the neutralino NLSP scenario. The cross-section limits in **a** are valid for any neutralino lifetime. Plot **b** shows the lifetimes at which the limit is set. The 95% C.L. cross-section limits for prompt neutralino decays, where only the search for photons, missing energy plus leptons/jets contributes, are plotted in **c**. In **d** the 95% C.L. cross-section limits are shown for very long-lived neutralinos, where only the search for acoplanar leptons contributes

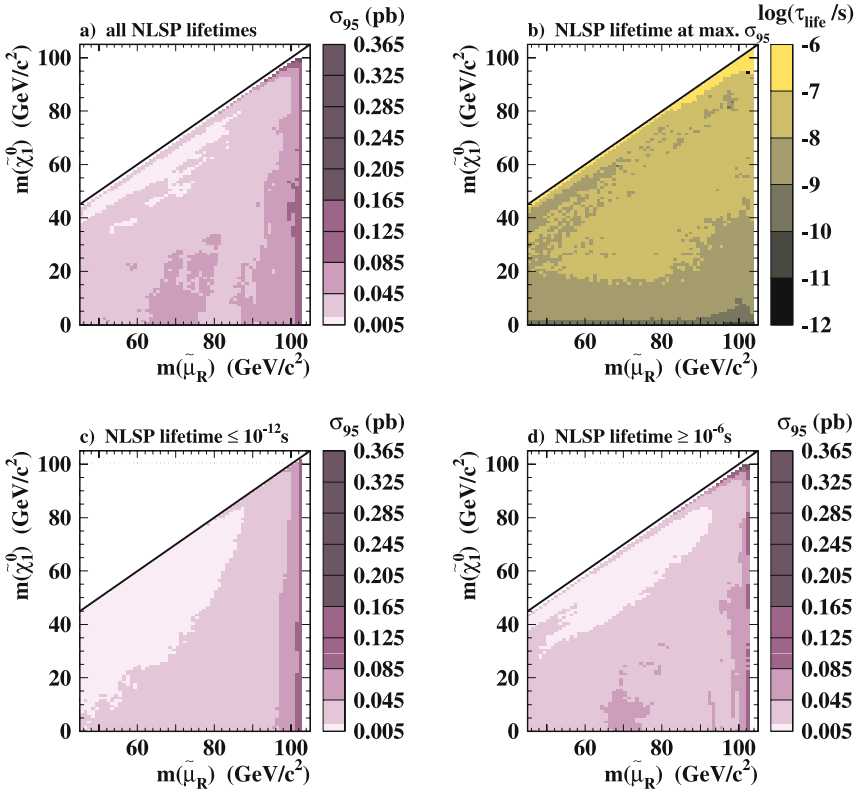

Fig. 16. Contours of the cross-section limits at 95% C.L. and $\sqrt{s} = 208$ GeV for smuon pair-production in the neutralino NLSP scenario. The cross-section limits in **a** are valid for any neutralino lifetime. Plot **b** shows the lifetimes at which the limit is set. The 95% C.L. cross-section limits for prompt neutralino decays, where only the search for photons, missing energy plus leptons/jets contributes, are plotted in **c**. In **d** the 95% C.L. cross-section limits are shown for very long-lived neutralinos, where only the search for acoplanar leptons contributes

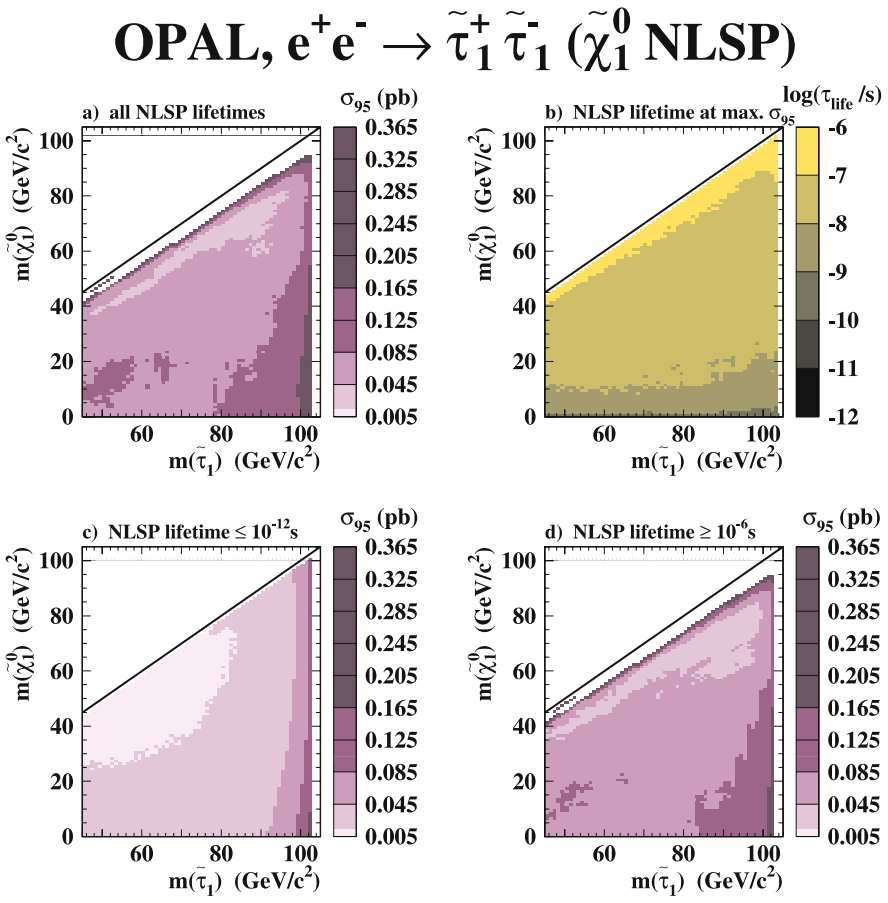

Fig. 17. Contours of the cross-section limits at 95% C.L. and $\sqrt{s} = 208$ GeV for stau pair-production in the neutralino NLSP scenario. The cross-section limits in **a** are valid for any neutralino lifetime. Plot **b** shows the lifetimes at which the limit is set. The 95% C.L. cross-section limits for prompt neutralino decays, where only the search for photons, missing energy plus leptons/jets contributes, are plotted in **c**. In **d** the 95% C.L. cross-section limits are shown for very long-lived neutralinos, where only the search for acoplanar leptons contributes

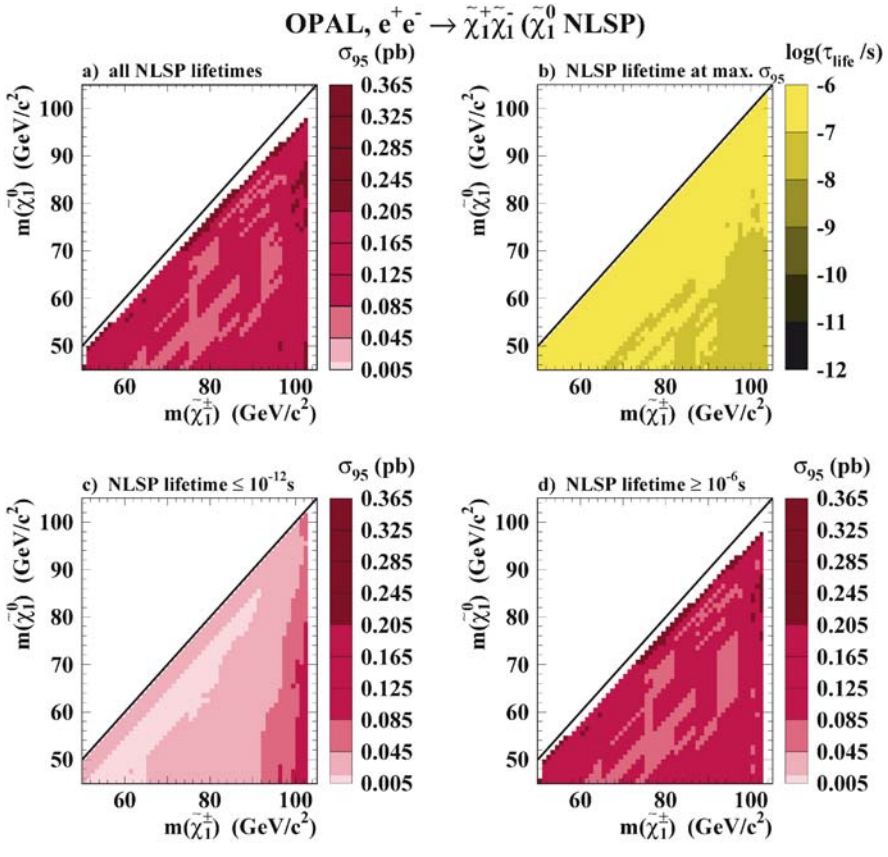

Fig. 18. Contours of the cross-section limits at 95% C.L. and $\sqrt{s} = 208$ GeV for chargino pair-production in the neutralino NLSP scenario assuming a 100% branching faction for $\tilde{\chi}^{\pm} \to W^{\pm *} \tilde{\chi}^0$. The cross-section limits in **a** are valid for any neutralino lifetime. Plot **b** shows the NLSP lifetimes at which the maximum excluded cross-section is found. The results for prompt neutralino decays, where mainly the searches for photons and missing energy plus leptons/jets contribute, are plotted in **c**. In **d** the limits are shown for very long-lived neutralinos

Table 4. Scanned points in the GMSB parameter space. The parameter Λ sets the overall mass scale of the SUSY particles, $\tan\beta$ is the ratio of the vacuum expectation values of the two Higgs doublets, M is the messenger scale, N the messenger index, and sign(μ) is the sign of the Higgs sector mixing parameter

Parameter	Scan points	Step size
Λ	5 – 150 TeVc^2	1 TeV/c^2
$\tan\beta$	1 – 50	0.2
M	$1.01\cdot\Lambda$, 250 TeV/c^2, 10.6 TeV/c^2	
N	1, 2, 3, 4, 5	
sign(μ)	+1, −1	
M_{top}	175 GeV/c^2	

is motivated by the requirement that the branching ratio of the next-to-NLSP to the gravitino is small and only the NLSP decays to the gravitino. As long as this is fulfilled, the cross-sections and branching ratios do not depend on the gravitino mass. This makes it possible to decouple the issue of NLSP lifetime, which depends on $\sqrt{F}$, from the scan. Note that $\sqrt{F}$ does not have a large effect on the other sparticle masses.

7.2 Direct constraints on the NLSP mass (stau or slepton)

Constraints on the NLSP masses were determined from the cross-section limits obtained for NLSP pair-production in the slepton co-NLSP scenario and stau pair-production in the stau NLSP scenario (Sect. 6.1.1). This was done by comparing the excluded cross-section at $\sqrt{s} = 208$ GeV with the production cross-section predicted by the theory. For pair-produced particles the expected cross-section times the branching ratio squared, $\sigma\cdot\mathrm{BR}^2$, within the model has to be known, but naturally this varies strongly within the model, depending on the parameter set chosen. To obtain values which are valid for each of the parameter sets considered, the following, conservative, minimization procedure was applied.

For each of the 30 parameter combinations of M, N and sign(μ), a scan over the parameters Λ and $\tan\beta$ was performed. In the regions where the sleptons or stau are the NLSP the minimum $\sigma\cdot\mathrm{BR}^2$ for each NLSP mass is determined within the parameter set considered. For selectrons strong variations were found because of additional positive and negative interfering t-channel production which contributes differently for the various parameter sets. This is in constrast to selectron searches in gravity mediated SUSY models in which the selectron cross-section is always enhanced by an interfering t-channel contribution. Finally for each NLSP mass the minimum of $\sigma\cdot\mathrm{BR}^2$ within these 30 scenarios was calculated and the resulting minimal expected cross-sections were compared to the experimentally achieved limit.

Figure 19 shows the mass limits for staus in the stau NLSP scenario (a), and smuons and selectrons in the slepton co-NLSP scenario (b,c) as a function of their lifetime. For each slepton flavour, the lowest mass constraints are found for very short slepton lifetimes, with the exception of the selectrons, where the region around 60 GeV/c^2 cannot be excluded at long lifetimes. This is due to the effect of similar values of the ionization energy loss of heavy and light charged particles for a region of momenta around 65 GeV/c, thus a decreased efficiency of the searches using the $\mathrm{d}E/\mathrm{d}x$ measurements. In the stau NLSP scenario, staus with masses below 87.4 GeV/c^2 are excluded at 95% C.L. for an expected limit from the background-only hypothesis of $m_{\tilde{\tau}_1} > 87.6$ GeV/c^2. In the slepton co-NLSP scenario the directly excluded selectron, smuon and stau masses (and expected limits), valid for any slepton lifetime, are $m_{\tilde{\mathrm{e}}_\mathrm{R}} > 60.1$ GeV/c^2 (60.0 GeV/c^2), $m_{\tilde{\mu}_\mathrm{R}} > 93.7$ GeV/c^2 (93.6 GeV/c^2) and $m_{\tilde{\tau}_1} > 87.4$ GeV/c^2 (88.2 GeV/c^2). In the slepton co-NLSP scenario the sleptons are mass-degenerate; their mass difference is – by definition – less than the τ, μ or e mass, so that decays $\tilde{\ell}' \to \ell'\tilde{\ell}$ are forbidden. Therefore the highest mass limit, the limit on the smuon mass of $m_{\tilde{\mu}_\mathrm{R}} > 93.7$ GeV/c^2 can be used to deduce an indirect common mass limit on all sleptons of $m_{\tilde{\ell}} = m_{\tilde{\mu}_\mathrm{R}} - M_\tau > 91.9$ GeV/c^2 within the slepton co-NLSP scenario.

No direct mass limits were calculated for SUSY particles heavier than the NLSP. The expected production cross-section for neutralinos, charginos, heavy selectrons or smuons depends strongly on the model parameters and is suppressed in some regions of the parameter space. Thus the minimization method gives no sensible general expectation which can be compared to the experimental results.

7.3 Direct constraints on the NLSP mass (short-lived neutralino)

For the neutralino NLSP, the same minimization method described in the previous section (Sect. 7.2) was applied to obtain an expected production cross-section valid at each scan point. In Fig. 14 this prediction is compared to the experimentally excluded production cross-section for neutralino pairs at a centre-of-mass energy of $\sqrt{s} = 208$ GeV. Neutralino masses less than 96.8 GeV/c^2 can be excluded at 95% C.L. for an expected limit from the background-only hypothesis of 96.3 GeV/c^2. The limit is valid for short-lived neutralinos with lifetimes up to 10^{-9} s only.

In the neutralino NLSP scenario no direct mass limits were computed for charginos and sleptons. The production cross-sections of these particles depend strongly on the model parameters and reach zero in some parts of the GMSB parameter space. Thus no general minimal expectation can be computed to compare to the experimental results.

7.4 Exclusions within the GMSB parameter space

For each of the 30 sets of the GMSB parameters N, M and sign(μ) considered in the scan, the exclusion in the Λ–$\tan\beta$ plane was studied. At each point in the plane, the cross-sections for the various channels as well as their branching

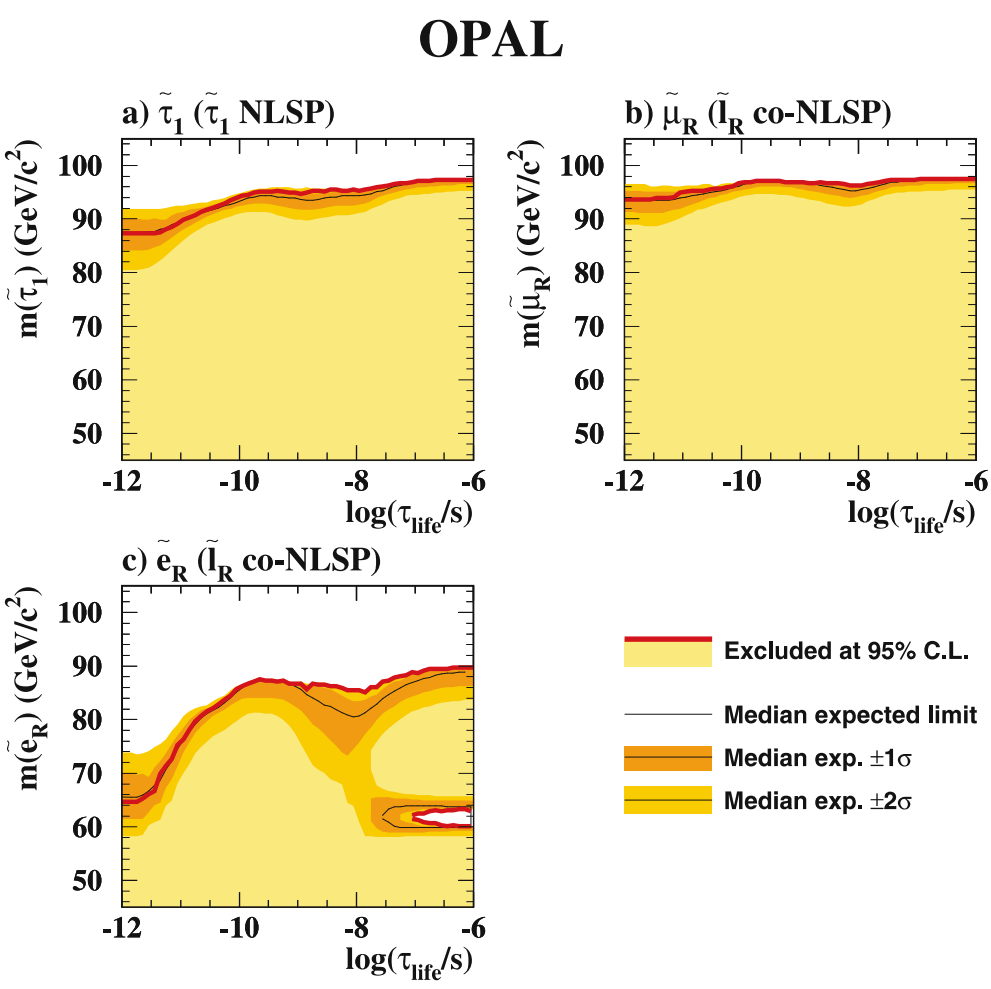

Fig. 19. The observed lower mass limits for pair-produced staus in the stau NLSP **a** and smuons **b**, selectrons **c** in the slepton co-NLSP scenario as a function of the particle lifetime using the direct $\tilde{\ell}^+\tilde{\ell}^-$ search. The observed limits are represented by *thick lines*, the *light grey regions* below are excluded at 95% Confidence Level. The *thin lines* represent the median expectations. The 95% and 68% probability intervals, centred on the median, are shown as *dark* and *medium grey bands*, respectively. For staus in the slepton co-NLSP scenario the observed and expected lower limit are identical to the limits of the stau in the stau NLSP scenario. The mass limits are valid for a messenger index N$\leq$ 5. For the stau NLSP and slepton co-NLSP scenarios, the NLSP mass limits are set by the stau mass limit ($m_{\mathrm{NLSP}} > 87.4\,\mathrm{GeV}/c^2$ **a**) and by the smuon mass limit ($m_{\mathrm{NLSP}} > 93.7\,\mathrm{GeV}/c^2$ **b**), respectively

ratios are known. A point in the parameter space is excluded if it is kinematically accessible and the expected cross-section in at least one channel is higher than the experimentally derived 95% C.L. cross-section limit in this channel, taking into account the branching ratio(s).

As examples, in Fig. 20 the excluded regions in the Λ–$\tan\beta$ plane, valid for any NLSP lifetime, are shown for $N = 1$ and 3, $M = 1.01 \cdot \Lambda$ and 250 TeV/c^2 and sign(μ) > 0. The shaded or hatched regions correspond to different search channels, indicating the relevance of the various analyses in the parameter space.

In general, the stau NLSP and slepton co-NLSP scenarios become more important as number of messenger sets N increases. Searches for direct NLSP pair-production exclude almost completely the accessible region of the stau NLSP and slepton co-NLSP scenarios. Only a few additional points are excluded by the neutralino searches, for example regions with $\tan\beta \approx 12$ and $\Lambda \approx 55\,\mathrm{TeV}/c^2$ for $N = 1$, $M = 1.01 \cdot \Lambda$ in Fig. 20.

The neutralino NLSP scenario plays an important role only for $N = 1$ and in regions with high M for $N = 2$. In this scenario, a large fraction of the parameter space can be excluded by searches for slepton pair-production. Searches for chargino pair-production exclude additional points in regions with low $\tan\beta$ and high M. In the chargino channel a complication arises due to the fact that the chargino has two decay modes which can lead to the same final state:

(1) $e^+e^- \to \tilde{\chi}_1^+\tilde{\chi}_1^- \to \tilde{\chi}_1^0 W^{+*}\tilde{\chi}_1^0 W^{-*} \to \tilde{\chi}_1^0\ell^+\nu\tilde{\chi}_1^0\ell^-\bar{\nu}$,
(2) $e^+e^- \to \tilde{\chi}_1^+\tilde{\chi}_1^- \to \ell^+\nu\tilde{\ell}^-\bar{\nu} \to \ell^+\nu\tilde{\chi}_1^0\ell^-\bar{\nu}\tilde{\chi}_1^0$.

Since in the scan for the branching ratios of the different final states no information about the decay chain is available, it is impossible to decide if the branching ratio to the $\ell^-\bar{\nu}\ell^+\nu$ final state is due to leptonic W decays (1), or due to the direct decay mode (2). For the interpretation, only results from the decay channel (1) were used. The analyses sensitive to the leptonic final state are the search for acoplanar leptons in case of long neutralino lifetimes and the search for photons, missing energy plus leptons for short lifetimes. It was checked that these analyses have a similar efficiency for both chargino decay modes that lead to the leptonic final state. The branching ratio to $\ell\nu$ was treated as if it was purely due to channel (1). Since the efficiency for (2) is the same, even if this branching ratio was totally due to decay mode (2), the cross-section limits would not be affected.

In general, the production cross-section for charginos is larger than that for sleptons in the regions excluded by this channel. Nevertheless, the slepton searches exclude larger regions than chargino searches because in GMSB models

charginos are mostly heavier than the (right-handed) sleptons. Thus, the charginos are kinematically limited and higher values of Λ can be reached by the slepton searches.

7.5 Constraints on the SUSY particle mass scale Λ

From the exclusions in the Λ–$\tan\beta$ plane for each of the 30 sets of the GMSB parameters N, M and $\mathrm{sign}(\mu)$ considered in the scan, lower limits were inferred on the SUSY particle mass scale Λ, independent of $\tan\beta$. For fixed N, the parameter Λ determines the GMSB particle spectrum at the messenger scale, since the gaugino masses are given by $m_{\lambda_i}(M) \sim N \cdot \Lambda \cdot \alpha_i(M)/4\pi$, where λ_i are the gaugino fields of gauge group i and the α_i are the GUT-scale normalized coupling constants of these gauge groups. The scalar masses at the messenger scale are determined by $m^2(M) \sim 2N \cdot \Lambda^2 \sum_{i=1}^{3} k_i \left(\alpha_i(M)/4\pi\right)^2$, where the sum is over the gauge groups $SU(3)_C$, $SU(2)_L$ and $U(1)_Y$, and k_i are constants of $\mathcal{O}(1)$.

The results, valid for all NLSP lifetimes and thus independent of the SUSY breaking scale $\sqrt{F}$, are summarized in Table 5. It can be seen that the constraints on Λ decrease with larger N and lower limits of typically $40\,\mathrm{TeV}/c^2$ are found for $N = 1$ and $15\,\mathrm{TeV}/c^2$ for $N = 5$. The constraints

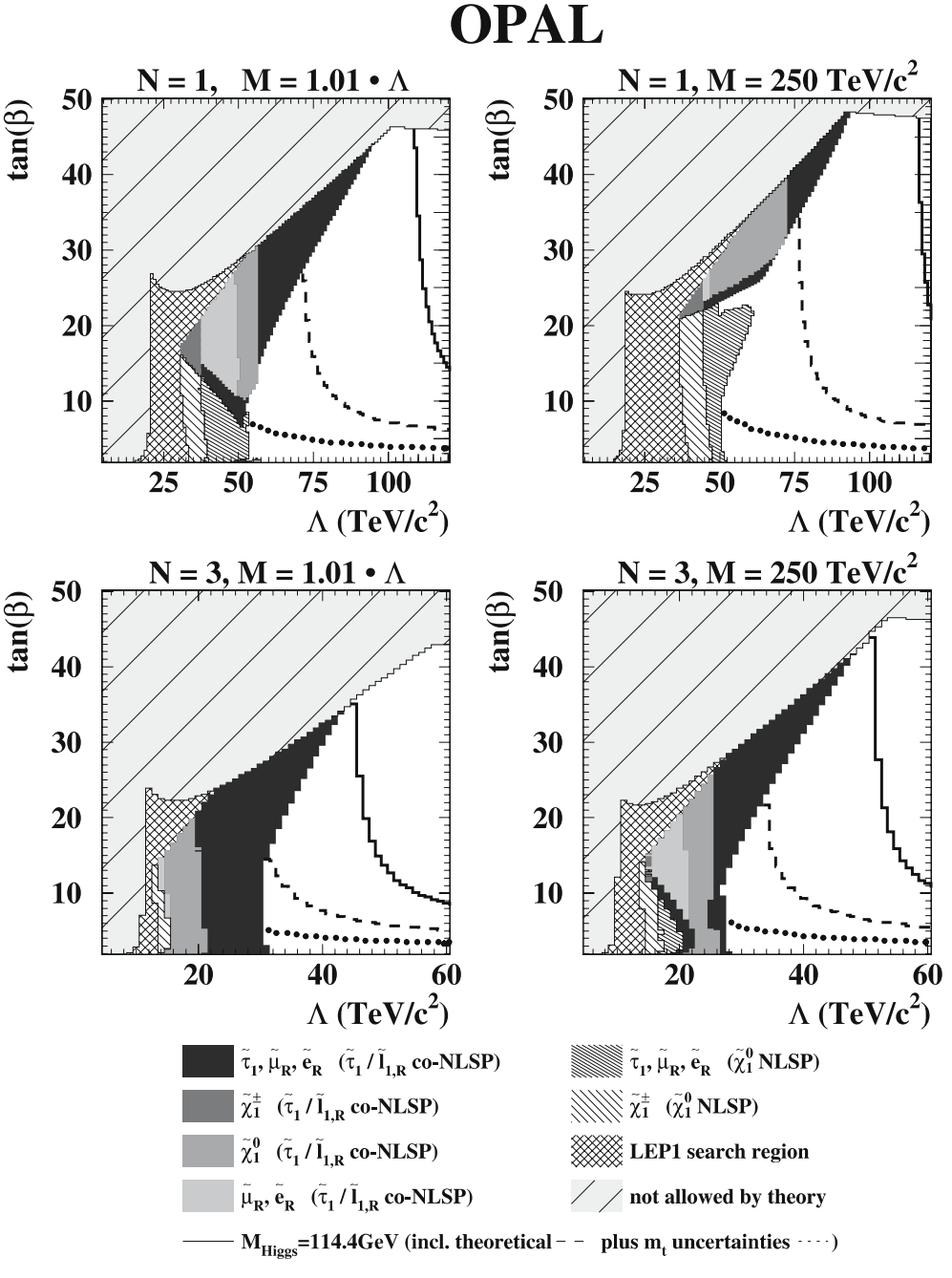

Fig. 20. Examples of regions in the $\Lambda - \tan\beta$ plane excluded by pair-production searches for different particles, with $\mathrm{sign}(\mu) > 0$ and valid for any NLSP lifetime for four different sets of parameters, $N = 1$ or 3 and $M = 1.01 \cdot \Lambda$ or $250\ \mathrm{TeV}/c^2$. The *light grey regions* with positive hatching are not allowed by theory. In the *cross-hatched regions* the NLSP is lighter than $45\,\mathrm{GeV}/c^2$. These regions were not considered in this analysis. The *white regions* cannot be excluded by the GMSB sparticle searches. Regions with a negative slope hatching are excluded by searches for charginos (*large hatch spacing*) and sleptons (*small spacing*) in the neutralino NLSP scenario. The *filled areas* are excluded by searches in the stau NLSP or slepton co-NLSP scenario. The *darkest grey regions* are excluded by searches for direct NLSP production, next-dark grey regions by chargino searches, then regions by neutralino searches and the lightest grey indicates regions excluded by selectron/smuon pair-production in stau NLSP scenario. The *solid line* indicates the region in which the Higgs mass is below 114.4 GeV; the *dashed line* illustrates the effect of the 3 GeV theoretical uncertainty on the determination of the Higgs mass in GMSB, and the *dotted line* illustrates the additional effect of the 5 GeV uncertainty on the Higgs mass determination due to the uncertainty in M_{top}

Table 5. Lower limits at 95% C.L. on the SUSY particle mass scale Λ, for various sets of the GMSB parameters M, N and sign(μ), valid for all NLSP lifetimes These constraints use only the direct searches for SUSY particle production. The minimum value of Λ for each N is highlighted

		Lower limit at 95% C.L. on Λ [TeV/c^2] for all NLSP lifetimes				
		$N=1$	$N=2$	$N=3$	$N=4$	$N=5$
High M ($M = 10^6$TeV/c^2)	$\mu<0$	**40**	**27**	**21**	**17**	**15**
	$\mu>0$	43	**27**	**21**	**17**	**15**
Medium M ($M = 250$ TeV/c^2)	$\mu<0$	49	31	26	22	20
	$\mu>0$	49	34	26	22	20
Low M ($M = 1.01\Lambda$)	$\mu<0$	54	37	30	25	22
	$\mu>0$	52	37	30	25	22

depend on M, but are almost independent of sign(μ). The limits are set at values of tan β between 5 and 25; for higher and lower tan β values they get larger. In conclusion, constraints on Λ of $\Lambda > 40$, 27, 21, 17, 15 TeV/c^2 were derived for $N = 1$, 2, 3, 4, 5, respectively, for all M, tan β, sign(μ) and all NLSP lifetimes (all values of $\sqrt{F}$).

The constraints on Λ imply a lower limit on the neutralino mass in the neutralino NLSP scenario, independent of the neutralino lifetime. Masses below 53.5 GeV/c^2 for $N = 1$ up to 94.0 GeV/c^2 for $N = 5$ can be excluded for all neutralino lifetimes.

7.6 Impact of searches for the neutral Higgs boson

The limit on the standard model Higgs boson reached by the four LEP experiments [32] can be used to place additional constraints on the GMSB parameter space. This is justified as in GMSB there is almost no parameter space in which the Higgs–Z–Z coupling is suppressed compared to its standard model value. Also, in GMSB the branching ratio of $H \to b\bar{b}$, the most important channel in the SM Higgs search, shows no strong dependence on tan β and is suppressed by at most 10% in a few regions of the phase space [33].

In Fig. 20, in addition to the regions excluded by direct sparticle searches, constraints from the LEP combined Higgs limit of 114.4 GeV/c^2 are also shown. The Higgs constraints initially appear to be much stronger than those from the direct SUSY particle searches; however, for a given set of GMSB parameters, the theoretical uncertainty on the inferred Higgs mass is about 3 GeV/c^2, and the Higgs mass uncertainty due to the uncertainty on $M_{\rm top}$ is about 5 GeV/c^2 [33]. The effect of these uncertainties is also illustrated in Fig. 20, where it can be seen that the Higgs constraints can be rather weak when the full uncertainty is taken into account. Because of these large uncertainties, constraints on the GMSB parameter space from the Higgs search are not included in our quoted limits.

8 Conclusions

Searches have been performed for topologies predicted by GMSB models. All possible lifetimes of the NLSP which is either the lightest neutralino or a slepton, have been considered.

No evidence for new physics has been found in the OPAL data sample collected at centre-of-mass energies up to $\sqrt{s} = 209$ GeV. For the first time limits are presented on the production cross-section for all search topologies. The impact of the searches on the minimal GMSB model has been tested by performing a scan over its parameters. NLSP masses below 53.5 GeV/c^2 in the neutralino NLSP scenario, below 87.4 GeV/c^2 in the stau NLSP scenario and below 91.9 GeV/c^2 in the slepton co-NLSP scenario can be excluded at 95% C.L. for all lifetimes of the NLSP. The scan gives constraints on the universal SUSY mass scale Λ from the direct searches for SUSY particle production of $\Lambda > 40$, 27, 21, 17, 15 TeV/c^2 for $N = 1$, 2, 3, 4, 5 for all NLSP lifetimes.

Acknowledgements. We particularly wish to thank the SL Division for the efficient operation of the LEP accelerator at all energies and for their close cooperation with our experimental group. In addition to the support staff at our own institutions we are pleased to acknowledge the Department of Energy, USA, National Science Foundation, USA, Particle Physics and Astronomy Research Council, UK, Natural Sciences and Engineering Research Council, Canada, Israel Science Foundation, administered by the Israel Academy of Science and Humanities, Benoziyo Center for High Energy Physics, Japanese Ministry of Education, Culture, Sports, Science and Technology (MEXT) and a grant under the MEXT International Science Research Program, Japanese Society for the Promotion of Science (JSPS), German Israeli Bi-national Science Foundation (GIF), Bundesministerium für Bildung und Forschung, Germany, National Research Council of Canada, Hungarian Foundation for Scientific Research, OTKA T-038240, and T-042864, The NWO/NATO Fund for Scientific Research, the Netherlands.

References

1. H.P. Nilles, Phys. Rep. **110**, 1 (1984)
2. G.F. Giudice, R. Rattazzi, Phys. Rep. **322**, 419 (1999)
3. S. Ambrosanio, G.D. Kribs, S.P. Martin, Phys. Rev. D **56**, 1761 (1997)
4. S. Dimopoulos, S. Thomas, J.D. Wells, Nucl. Phys. B **488**, 39 (1997)

5. S. Deser, B. Zumino, Phys. Rev. Lett. **38**, 1433 (1977)
6. A. De Gouvêa, T. Moroi, H. Murayama, Phys. Rev. D **56**, 1281 (1997)
7. OPAL Collaboration, G. Abbiendi et al., Eur. Phys. J. C **32**, 453 (2004)
8. OPAL Collaboration, G. Abbiendi et al., Phys. Lett. B **572**, 8 (2003)
9. OPAL Collaboration, G. Abbiendi et al., Phys. Lett. B **602**, 167 (2004)
10. OPAL Collaboration, G. Abbiendi et al., Eur. Phys. J. C **35**, 1 (2004)
11. OPAL Collaboration, K. Ahmet et al., Nucl. Instrum. Methods A **305**, 275 (1991)
12. S. Anderson et al., Nucl. Instrum. Methods A **403**, 326 (1998)
13. OPAL Collaboration, G. Abbiendi et al., Eur. Phys. J. C **33**, 173 (2004)
14. S. Katsanevas, P. Morawitz, Comput. Phys. Commun. **112**, 227 (1998)
15. C. Dionisi et al., in 'Physics at LEP2', ed by G. Altarelli, T. Sjöstrand, F. Zwirner, CERN 96-01, **2**, 337 (1996)
16. T. Sjöstrand, Comput. Phys. Commun. **82**, 74 (1994); Comput. Phys. Commun. **112**, 227 (1998)
17. R. Brun et al., GEANT3, CERN–DD/EE/84–1, 175 (1987)
18. F.A. Berends, P.H. Daverveldt, R. Kleiss, Comput. Phys. Commun. **40**, 271 (1986); Nucl. Phys. B **253**, 421 (1985)
19. J.A.M. Vermaseren, Nucl. Phys. B **229**, 347 (1983)
20. E. Boudinov et al., "$\gamma\gamma$ Event Generators" (1995) hep-ph/9512371
21. G. Marchesini et al., Comput. Phys. Commun. **67**, 465 (1992)
22. S. Jadach et al., Comput. Phys. Commun. **119**, 272 (1999)
23. J. Fujimoto et al., Comput. Phys. Commun. **100**, 128 (1997).
24. F.A. Berends, R. Kleiss, Nucl. Phys. B **186**, 22 (1981)
25. S. Jadach, W. Placzek, B.F.L. Ward, Phys. Lett. B **390**, 298 (1997)
26. D. Karlen, Nucl. Phys. B **289**, 23 (1987)
27. S. Jadach, B.F.L. Ward, Z. Wąs, Comput. Phys. Commun. **130**, 260 (2000)
28. G. Montagna, O. Nicrosini, F. Piccinini, Comput. Phys. Commun. **98**, 206 (1996)
29. OPAL Collaboration, K. Ackerstaff et al., Eur. Phys. J. C **2**, 213 (1998)
30. N. Brown, W.J. Stirling, Phys. Lett. B **252**, 657 (1990); S. Bethke, Z. Kunszt, D. Soper, W.J. Stirling, Nucl. Phys. B **370**, 310 (1992); S. Catani et al., Phys. Lett. B **269**, 432 (1991); N. Brown, W.J. Stirling, Z. Phys. C **58**, 629 (1992)
31. T. Junk, Nucl. Instrum. Methods A **434**, 435 (1999)
32. ALEPH, DELPHI, L3 and OPAL Collaboration, R. Barate et al., Phys. Lett. B **565**, 61 (2003)
33. S. Ambrosanio, A. Dedes, S. Heinemeyer, S. Su, G. Weiglein, Nucl. Phys. B **624**, 3 (2002)